Increased reluctant vesicles underlie synaptic depression by GPR55 in axon terminals of cerebellar Purkinje cells

Takuma Inoshita[1] and Shin-ya Kawaguchi[1,*]

[1] Department of Biophysics, Graduate School of Science, Kyoto University
Oiwake-cho, Kitashirakawa, Sakyo-ku, Kyoto, 606-8502, Japan

*: Correspondence should be addressed to S. K.
e-mail: kawaguchi@nb.biophys.kyoto-u.ac.jp
Tel: 81-75-753-4200

Running Title
Synaptic suppression by GPR55 distinct from conventional CBRs

Keywords
cannabinoid, synaptic suppression, GPR55, synapse, Purkinje cell

Abstract

Control of synaptic transmission efficacy by neuronal activity and neuromodulators is pivotal for brain function. Synaptic suppression by cannabinoids activating CB1 receptors has been extensively studied at the molecular and cellular levels to understand the neuronal basis for effects of cannabis intake. Here, we focused on GPR55, non-canonical type of cannabinoid receptor, which shows sensitivity to cannabidiol included in cannabis, aiming to highlight its actions on presynaptic function. Taking advantage of direct patch-clamp recordings from axon terminals of cerebellar Purkinje cells together with fluorescent imaging of vesicular exocytosis using synapto-pHluorin, we show that GPR55 suppresses synaptic transmission as CB1 receptor does, but through a distinct presynaptic modulation of release machinery. Activation of GPR55 reduced transmitter release by changing neither presynaptic action potential waveform nor Ca^{2+} influx, but by making a large population of Ca^{2+}-responsive synaptic vesicles insensitive to Ca^{2+} influx through voltage-gated Ca^{2+} channels, leading to substantial reduction of the readily releasable pool of vesicles. Thus, the present study identifies a unique mechanism to suppress presynaptic transmitter release by an atypical cannabinoid receptor GPR55, which would enable subtype-specific modulation of neuronal computation by cannabinoid receptors.

Introduction

Neuronal communication at chemical synapses is central to information processing in the circuit, and its activity-dependent modulation provides adaptive change of brain computation (Kandel, 2001). Short- and long-term changes of transmission efficacy at central synapses have been extensively studied in terms of molecular/cellular mechanisms and physiological significance, which have demonstrated their critical roles in learning and memory in animals (Abbott and Regehr, 2004). One of such modulations of synaptic strength is that by endocannabinoids (Kreitzer and Regehr, 2001; Ohno-Shosaku et al., 2001; Wilson and Nicoll, 2001; Diana et al., 2002), which is also related to the cellular and neuronal basis for actions of cannabis (Kano et al., 2009). One well-known synaptic modulation by cannabinoids is the activity-dependent short-term suppression of synaptic transmission, such as depolarization-induced suppression of excitation (DSE) and inhibition (DSI), caused by reduced transmitter release from presynaptic terminals as a result of activation of cannabinoid receptor type 1 (CB1). The CB1 receptor activation is thought to decrease presynaptic Ca^{2+} influx upon an action potential (AP) arrival (Kreitzer and Regehr, 2001; Kushmerick et al., 2004; Wu et al., 2020).

In spite of the substantial efforts that have been made for unraveling cannabinoids' action on the nervous system, it still remains elusive whether the reduction of Ca^{2+} influx fully explains the suppression of transmission by cannabinoids or other mechanisms, such as altered release machinery, may also be involved generally at central synapses, as already suggested for CB1-mediated change of presynaptic vesicular docking (Ramirez-Franco et al., 2014). In addition, multiple types of molecules contained in cannabis are now known to act on the nervous system, and particularly one of them, cannabidiol, is attracting attention because of its potential preferred therapeutic actions on various neurological dysfunctions such as epilepsy and anxiety symptoms (Shallcross et al., 2019; Devinsky et al., 2024). GPR55, a cannabinoid receptor that has been identified as a potential target of cannabidiol (Baker et al., 2006; Oka et al., 2007), was recently reported to modulate synaptic transmission at glutamatergic and GABAergic synapses in the hippocampus (Sylantyev et al., 2013; Rosenberg et al., 2023), although the detailed mechanism of action remains unclear. GPR55, unlike typical cannabinoid receptors such as CB1 receptors that couple to G_i proteins, interacts with multiple G proteins including $G\alpha_q$ and $G\alpha_{13}$, thereby activating downstream pathways such as phospholipase C (PLC)/IP_3-mediated Ca^{2+} signaling and RhoA/ROCK-dependent cytoskeletal modulation (Henstridge et al., 2010; Balenga et al., 2011). This distinct signaling profile suggests that GPR55 is likely to regulate synaptic transmission through a mechanism different from CB1 receptor.

To study in detail how cannabinoids modulate synaptic physiology, direct *tour-de-force* patch-clamp recording of transmitter release at axon terminals, in combination with molecular biological methods and fluorescent imaging, would be a powerful technique. One preparation that is amenable to detailed biophysical analysis of transmitter release is the axon terminals of cerebellar Purkinje cells

(PCs) (Kawaguchi and Sakaba, 2015), which are expected to express GPR55 based on data from in situ hybridization, RT-PCR and immunolabeling (Ryberg et al., 2007; Wu et al., 2013), although its subcellular localization remains unclear. Taking advantage of the feasibility to perform direct patch-clamp recording from axon terminals in combination with fluorescent imaging of vesicular fusion in dissociated cultures, and postsynaptic recordings from neurons in deep cerebellar nuclei (DCN) of slices, here we studied how the presynaptic release machinery is modulated by GPR55. Here, we demonstrate that GPR55 is present at PC axon terminals and suppresses synaptic transmission through a unique modulatory action: GPR55 increases reluctant vesicles by depriving the sensitivity to APs.

Results

GPR55 inhibits synaptic transmission at PC output synapses

We first examined the role of GPR55 in synaptic transmission from a PC in acute cerebellar slices. Cerebellar sagittal slices were prepared from postnatal day (P)28-35 rats, and whole-cell patch-clamp recordings were performed from neurons with large cell bodies (> 15 μm diameter) in the DCN (Figure 1A; Uusisaari et al., 2006). The DCN neurons were voltage-clamped at -70 to -100 mV, and evoked IPSCs (eIPSCs) were recorded following electrical stimulation at the white matter in the presence of an AMPA receptor antagonist, NBQX (10 μM). In accord with previous studies (Kawaguchi and Sakaba, 2015), eIPSCs at PC-DCN synapses were identified by the sudden appearance of large amplitude responses (2.04 ± 0.48 nA) in an almost all-or-none manner as stimulation intensity was increased (Figure 1B). Bath application of a GPR55 agonist, AM251 (5 μM; EC_{50} = 39 nM assayed in HEK cells; Ryberg et al., 2007; Henstridge et al., 2009) decreased the amplitude of eIPSCs (69.1 ± 5.1% at +5 min, p = 0.00226, compared with -1 min, paired t-test), accompanied by an increase in the coefficient of variation (CV) of the responses (156.0 ± 19.8% at +5 min, p = 0.0490) (Figure 1B, C). Increase in the CV is typically interpreted as a lowered presynaptic release probability. These results suggest that GPR55 suppresses synaptic transmission at PC-DCN synapses, similarly to what CB1 receptor does at other synapses (Kreitzer and Regehr, 2001; Ohno-Shosaku et al., 2001; Wilson and Nicoll, 2001; Diana et al., 2002). Aiming at much more detailed analysis of synaptic function based on the feasibility to perform direct patch-clamp recordings from axon terminals, we also tested the action of GPR55 on PC outputs using the primary culture preparation. To fluorescently visualize PCs, we used an adeno-associated virus (AAV) vector, AAV2-CA-EGFP that preferentially infects PCs among cerebellar neurons, as in previous studies (Kawaguchi and Sakaba, 2015). Simultaneous whole-cell somatic patch-clamp recordings were performed from a presynaptic PC and its postsynaptic neuron (possible DCN neuron) surrounded by lots of EGFP-positive PC boutons, in the presence of NBQX (10 μM) (Figure 1D). Presynaptic PCs were voltage-clamped at -70 mV, and Na^+ current escaping as an AP from the patched soma to the axon was elicited by applying a voltage

110 pulse (to 0 mV, 1~5 ms), which evoked IPSCs in the voltage-clamped postsynaptic target cell. In line
111 with the data obtained in slices, synaptic transmission decreased upon GPR55 activation with AM251
112 (300 nM), manifested as a decrease in IPSC amplitudes (42.9 ± 8.0% at +5 min, p = 0.0134) and an
113 increase in the CV (147.6 ± 14.7% at +5 min, p = 0.0431) (Figure 1E, I). The effect of AM251 became
114 evident a few minutes after application, and somehow reached a saturated level within 5 minutes in
115 both slice and culture preparations. It should be noted that AM251 is known to act not only as a
116 GPR55 agonist, but also as an inverse agonist for CB1 (Ryberg et al., 2007; Henstridge et al., 2009).
117 To confirm that the effect of AM251 is not due to the CB1 receptor inhibition, we also tested AM281,
118 a CB1-specific inverse agonist. Application of AM281 (500 nM) did not induce any significant changes
119 in eIPSC amplitude or its CV (amplitude: 97.8 ± 3.6% at +5 min, p = 0.737; CV: 102.1 ± 7.5% at +5
120 min, p = 0.260) (Figure 1F, I), suggesting that the synaptic depression caused by AM251 is not due
121 to CB1 receptor inhibition. Considering a previous study showing that PC synapses exhibit no
122 modulation by CB1 receptors (Hirono and Yanagawa, 2021; see also Figure 1F, I), the effects of
123 AM251 on synaptic outputs from a PC bouton seemed to be ascribed to activation of GPR55. Indeed,
124 the suppressive effect of AM251 on synaptic transmission was abolished by a GPR55 antagonist
125 CID16020046 (CID, 5 μM; IC_{50} = 0.21 μM, specific for GPR55 without affecting CB1 receptor)
126 (amplitude: 101.9 ± 16.4% at +5 min, p = 0.949; CV: 104.1 ± 13.1% at +5 min, p = 0.624) (Figure 1G,
127 I). In addition, we also tested another GPR55 ligand, lysophosphatidylinositol (LPI, 1 μM; EC_{50} = 30
128 nM, Oka et al., 2007), which is known as an endogenous ligand of GPR55 (Oka et al., 2007;
129 Henstridge et al., 2009). Several types of LPI are known, and here we used soy-derived LPI (Merck,
130 containing approximately 58% C16:0 and 42% C18:0 or C18:2), which was shown to activate GPR55
131 for synaptic modulation in the hippocampus (Rosenberg et al., 2023). As shown in Figure 1H and I,
132 similar reduction of eIPSC amplitude and increase in its CV to those by AM251 were observed after
133 the extracellular application of LPI (amplitude: 57.2 ± 4.6% at +5 min, p = 0.00111; CV: 141.2 ± 3.6%
134 at +5 min, p = 0.00292). Neither application of AM251 nor LPI changed the time courses of IPSCs
135 (AM251, 20-80% risetime: 0.81 ± 0.05 to 0.77 ± 0.04 ms, p = 0.296; LPI, 0.71 ± 0.10 to 0.65 ± 0.12
136 ms, p = 0.222) (Figure 1—figure supplement 1A) and presynaptic Na^+ currents recorded at the PC
137 soma (AM251, 3.30 ± 0.33 to 3.25 ± 0.40 nA, p = 0.520; LPI, 2.87 ± 0.30 to 2.89 ± 0.31 nA, p = 0.728)
138 (Figure 1—figure supplement 1B, C). Taken all these results based on pharmacological agents for
139 GPR55 together, it was suggested that synaptic transmission is negatively regulated by GPR55 at
140 synapses formed by PC axon terminals, presumably acting on the presynaptic side.

141 It is a critical issue to examine the presence of GPR55 at PC axon terminals. To address this,
142 we attempted to fluorescently label neurons in cerebellar culture with molecules targeting GPR55,
143 using a fluorescent derivative of AM251, Tocrifluor T1117 (T1117; Daly et al., 2010; Sylantyev et al.,
144 2013; He et al., 2024). As shown in Figure 2A and B, confocal fluorescent images of GFP-positive PC
145 axons and terminals clearly showed significant T1117 signal after incubation with T1117 (20 nM) for
146 2 min, which was selectively suppressed by the CRISPR/Cas9-mediated acute knock-down of GPR55

147 expression (relative fluorescence density of T1117, mean ± SD: control, 1.00 ± 0.49; GPR55-KD, 0.53
148 ± 0.27, $p < 0.001$; Cas9-alone, 1.04 ± 0.47, $p = 0.493$, compared with control, Dunnett's test) (Figure
149 2C; see Methods for details of the CRISPR/Cas9 knock-down). Thus, T1117 signals at PC axon
150 terminals would be ascribed at least partially to GPR55. It should be noted that PC boutons showed
151 marked deviation in the T1117 fluorescence intensity, probably reflecting variable GPR55 abundance
152 at individual PC boutons. In addition, T1117 signals were also evident at GFP-negative structures
153 (see Figure 2), probably due to labeling of axons/terminals of neurons such as granule cells and
154 inhibitory interneurons which are well-known to potently express CB1 (Tsou et al., 1998), which is
155 antagonized by AM251. Indeed, GFP-negative structures neighboring the GPR55-knocked down
156 GFP-positive PC boutons showed clear T1117 signals (Figure 2B, C). The above results showing PC
157 terminals labeled with a fluorescent AM251 analogue depending on the GPR55 gene expression
158 indicated the presence of GPR55 with variable density at individual PC boutons, supporting the idea
159 about modulation of PC output synapses by GPR55 (see Figure 1).
160
161 **GPR55 suppresses transmitter release in PC boutons without changing presynaptic Ca^{2+}**
162 **influx**
163 Taking advantage of the feasibility to directly patch-clamp record from GPR55-expressing PC
164 axon terminals (Kawaguchi and Sakaba, 2015), we next attempted to examine the mechanism how
165 GPR55 suppresses the transmission. One candidate mechanism is the reduction of the presynaptic
166 Ca^{2+} influx, as CB1 does at the calyx of Held synapses and climbing fiber synapses on PCs (Kreitzer
167 and Regehr, 2001; Kushmerick et al., 2004; Wu et al., 2020). To record presynaptic Ca^{2+} current,
168 direct voltage-clamp recordings were performed from PC boutons (Figure 3A). Concomitantly, we
169 also monitored the membrane capacitance (C_m) increase (ΔC_m) caused by the Ca^{2+} influx, which is
170 an indication of the amount of exocytosed synaptic vesicles. Unexpectedly, Ca^{2+} currents induced by
171 square depolarizing pulses (0 mV for 5 ms) were not affected by AM251 in the voltage-clamped PC
172 boutons (53.0 ± 5.6 to 52.4 ± 6.3 pA/pF, $p = 0.808$), whereas the resultant increase in C_m was
173 markedly diminished (22 ± 4 to 13 ± 2 fF/pF, $p = 0.0448$) (Figure 3B, C). This strong reduction of
174 vesicle exocytosis by AM251 was mediated by GPR55, as evidenced by its abolishment by the knock-
175 down of GPR55 expression using CRISPR/Cas9 system without any effects on presynaptic Ca^{2+} influx
176 (Figure 3D, E; Ca^{2+} current: Cas9 alone, 55.1 ± 9.8 to 54.7 ± 9.6 pA/pF, $p = 0.715$, paired t-test;
177 GPR55-KD, 56.7 ± 10.0 to 54.7 ± 9.8 pA/pF, $p = 0.176$; ΔC_m: Cas9 alone, 28 ± 1 to 15 ± 1 fF/pF, $p <$
178 0.001; GPR55-KD, 27 ± 5 to 24 ± 6 fF/pF, $p = 0.174$). Taken together, our direct patch-clamp
179 recordings from PC terminals indicated potent suppression of vesicle exocytosis by GPR55 without
180 changing Ca^{2+} influx, which is distinct from the typical synaptic modulation by CB1 receptors through
181 a reduction of presynaptic Ca^{2+} influx.

182 We further tested whether GPR55 also affects APs and postsynaptic $GABA_A$ receptor
183 responsiveness at PC-DCN synapses. Previous studies demonstrated that AP waveforms are subject
184 to modulation in PC axons in a manner dependent on high frequency firing, local activation of axonal
185 transmitter receptors, and/or intracellular cAMP changes (Kawaguchi and Sakaba, 2015; Zorrilla de
186 San Martin et al., 2017; Furukawa et al., 2024). To test the possibility of a change in the AP waveform
187 by GPR55, we performed direct patch-clamp recordings of APs from a presynaptic bouton of a PC
188 axon (Figure 4A). As shown in Figure 4B and C, current-clamp recordings from the axon terminals
189 detected no changes of APs by GPR55 in both the amplitude and time course (amplitude: 91.2 ± 7.5
190 to 90.4 ± 6.4 mV, p = 0.701, paired t-test; half-width: 0.54 ± 0.06 to 0.54 ± 0.07 ms, p = 0.832). In
191 terms of modulation of postsynaptic responsiveness by GPR55, decrease in accumulation of
192 postsynaptic $GABA_A$ receptors at hippocampal GABAergic synapses was suggested (Khan A. et al.,
193 2018; Rosenberg et al., 2023). However, miniature IPSCs (mIPSCs) recorded from a postsynaptic
194 DCN cell innervated by lots of EGFP-labeled PC boutons in the presence of TTX (1 μM) and NBQX
195 (10 μM) (Figure 4D and Figure4—figure supplement 1) showed no change in either amplitude or
196 frequency after the AM251 application (amplitude: 101.5 ± 9.7% at +5 min, p = 0.941; frequency: 85.4
197 ± 13.4%, p = 0.608) (Figure 4E, F). Together, these results demonstrated that GPR55 suppresses
198 transmitter release from PC boutons not by altering presynaptic Ca^{2+} influx, AP waveforms, or
199 postsynaptic responsiveness, but rather by directly reducing vesicle exocytosis.
200
201 **GPR55 decreases the amount of vesicles in the readily-releasable pool**
202 To obtain insights into the mechanism of GPR55-mediated suppression of neurotransmitter
203 release, we biophysically analyzed the relation between presynaptic Ca^{2+} influx and vesicle
204 exocytosis by systematically changing depolarization pulses to a PC bouton. Depolarizing pulses with
205 different length altered the duration of presynaptic Ca^{2+} current, leading to distinct amounts of
206 vesicular release (Figure 5A). As summarized in Figure 5B, the Ca^{2+} current amplitude and its
207 activation kinetics were again not significantly affected by GPR55 activation (amplitude, p = 0.424;
208 tau, p = 0.339, ANOVA), supporting the idea that GPR55 does not affect the presynaptic Ca^{2+} influx.
209 On the other hand, ΔC_m induced by any duration of depolarization pulses showed ~50% reduction in
210 the presence of AM251 (31 ± 6 fF/pF and 15 ± 2 fF/pF upon 50 ms pulse without and with AM251,
211 respectively, p = 0.0289, Tukey-Kramer test) (Figure 5C, D). Thus, GPR55 halves the amount of
212 synaptic vesicles released within tens of milliseconds after a strong Ca^{2+} influx, corresponding to the
213 readily-releasable pool (RRP), presumably consisting of immediately releasable and slowly
214 releasable vesicles as in other boutons such as calyx of Held (Sakaba, 2006). The decrease of RRP
215 vesicles could be the primary cause for the decrease in AP-triggered synaptic transmission. We also
216 examined whether LPI, an endogenous agonist for GPR55, exerts a similar effect. When GPR55 was
217 activated by LPI, ΔC_m was smaller in size (17 ± 2 fF/pF upon 50 ms pulse, p = 0.0488, compared with

218 control, Tukey-Kramer test) to an extent of that by AM251, which was not enhanced by additional
219 application of AM251 (16 ± 4 fF/pF upon 50 ms pulse, p = 1.00, compared with LPI alone, Tukey-
220 Kramer test) (Figure 5—figure supplement 1). These results indicate that both LPI and AM251 act
221 through GPR55 and reduce the RRP.

222 Taking into consideration that the cytoplasm of PCs contains extremely potent Ca^{2+} buffering
223 capacity due to the large amount of calbindin (Fierro and Llano, 1996; Bornschein et al., 2013),
224 releasable vesicles in PC boutons might show steep dependency of their release competency on their
225 position relative to the voltage-gated Ca^{2+} channels (VGCCs). Previous studies reported that vesicular
226 fusion is insensitive to exogenous EGTA in the intracellular solution, a relatively slow but high-affinity
227 Ca^{2+} buffer, suggesting that vesicles tightly coupled to VGCCs are release-competent in PC boutons
228 (Kawaguchi and Sakaba, 2015; Diaz-Rojas et al., 2015). Indeed, the RRP size was comparable
229 between 0.5 and 5 mM cytoplasmic EGTA conditions (0.5 mM EGTA, 30 ± 5 fF/pF; 5 mM EGTA, 34
230 ± 4 fF/pF upon 50 ms pulse, p = 0.928, Tukey-Kramer test) (Figure 5C and Figure 5—figure
231 supplement 2). On the other hand, previous studies showed decrease in release by EGTA at
232 synapses with relatively loose coupling between VGCCs and releasable vesicles, such as squid giant
233 synapses, calyx of Held synapses, or hippocampal mossy fiber synapses (Adler et al., 1991; Borst
234 and Sakmann, 1996; Vyleta and Jonas, 2014). Therefore, if GPR55 loosens the Ca^{2+}-release
235 coupling, EGTA might become influential to the release even in PC boutons. However, the increase
236 in cytoplasmic EGTA from 0.5 to 5 mM did not reduce the apparent RRP size in PC boutons when
237 GPR55 was activated by AM251 (5 mM EGTA, 16 ± 3 fF/pF upon 50 ms pulse with AM251, p = 0.992,
238 compared to 15 ± 2 fF/pF with 0.5 mM EGTA and AM251, Tukey-Kramer test) (Figure 5C). Notably,
239 plotting the fold reduction of ΔC_m by AM251 against the duration of depolarization suggested that a
240 higher amount of EGTA augmented the suppressive effect of GPR55, particularly for the release in
241 response to short pulses (Figure 5D). This result implies that the reduction of release by GPR55 might
242 be somehow related to the Ca^{2+}-release coupling, although its extent is too small to be reflected as a
243 clear change of release sensitivity to EGTA. In summary, based on biophysical analysis of Ca^{2+}-
244 dependent release in terms of the modulations by GPR55 and cytoplasmic EGTA, we conclude that
245 the GPR55 activation reduces the amount of vesicles in the RRP, which might be accompanied by a
246 slight change of the functional coupling between release and Ca^{2+} influx.
247

248 **Slowed vesicular fusion by GPR55**

249 To further investigate the GPR55-mediated downregulation of vesicular fusion, the Ca^{2+}-
250 activated release kinetics were biophysically analyzed by simultaneous patch-clamp recordings from
251 both a presynaptic PC bouton and a postsynaptic cell. To avoid saturation of postsynaptic $GABA_A$
252 receptors, we applied a short depolarization pulse (0 mV, 2 ms) to the patched bouton, and recorded
253 presynaptic Ca^{2+} and postsynaptic currents (Figure 6A). In line with the above results, presynaptic
254 Ca^{2+} current showed little change by the AM251 administration (42.1 ± 7.9 to 44.8 ± 9.9 pA/pF, p =

255 0.332, paired t-test), while postsynaptic currents were clearly reduced by half (2.57 ± 0.97 to 1.38 ±
256 0.63 nA, p = 0.0448, paired t-test) (Figure 6A, B). By deconvolving the postsynaptic currents with the
257 template mIPSC trace, we estimated the temporal change of vesicular fusion velocity (for detail, see
258 Methods; Kawaguchi and Sakaba, 2015). The peak of vesicular fusion velocity was almost halved by
259 AM251 without a marked change of time course (45.7 ± 19.1 to 24.7 ± 11.3 vesicles/ms, p=0.0467,
260 paired t-test) (Figure 6C), showing similar reduction to that observed in the apparent RRP size
261 (vesicular fusion velocity: 46.9 ± 4.4%; ΔC_m: 48.4% upon 50 ms pulse shown in Figure 5D). Thus, it
262 would be reasonable to conclude that the RRP reduction, but not a change in the Ca^{2+}-activated
263 release probability, predominantly underlies the synaptic suppression induced by GPR55. However,
264 notably, AM251 induced a modest yet significant increase in synaptic delay, estimated by the time to
265 the onset of release (onset of vesicular release: 1.63 ± 0.20 to 2.08 ± 0.33 ms, p = 0.0403, paired t-
266 test) (Figure 6C). Thus, together with the idea that GPR55 somehow lowers the effectiveness of Ca^{2+}-
267 triggered release (as shown in Figure 5D), the apparent RRP reduction by GPR55 in PC boutons
268 might be caused by a process accompanied with a slight downregulation of the Ca^{2+}-mediated
269 activation process of vesicular fusion.
270
271 **Reduction of AP-sensitive vesicles by GPR55**
272 The above experiments demonstrated that GPR55 suppresses synaptic transmission
273 primarily by reducing the RRP size without altering Ca^{2+} influx at the presynaptic terminal. To
274 discriminate two possible causes for the decrease in RRP size: relative increase in the fraction of
275 reluctant vesicles or reduction of total vesicles present at the presynaptic terminal, we performed
276 fluorescence imaging of vesicular fusion with synapto-pHluorin expressed in PCs using AAV or
277 microinjection of plasmid DNA into the nucleus. First, APs were repetitively evoked (400 APs at 20
278 Hz) at the voltage-clamped PC soma by depolarization pulses triggering somatic Na^+ currents (Figure
279 7—figure supplement 1), and the fluorescence changes of pHluorin at axon terminals were monitored.
280 Synapto-pHluorin shows little fluorescence upon light illumination when its pH-sensitive fluorophore
281 is exposed to the acidic vesicular lumen, and becomes fluorescent after exocytosis through exposure
282 to the external neutral pH environment (Figure 7A), providing the sign of vesicle fusion as a
283 fluorescence increase (Sankaranarayanan and Ryan, 2000). As shown previously (Kawaguchi and
284 Sakaba, 2015), PC axonal varicosities exhibited synapto-pHluorin fluorescence increase by 23.3 ±
285 2.0% upon 400 APs at 20 Hz (Figure 7B-D). After the increase in fluorescence during the AP train
286 stimulation, pHluorin signal decayed with a time constant of about 40 sec, reflecting the endocytosis
287 of exocytosed synapto-pHluorin and the subsequent re-acidification of the vesicular lumen
288 (Nicholson-Tomishima and Ryan, 2004; Yamashita et al., 2018). In accord with the GPR55-mediated
289 reduction of synaptic transmission (see Figure 1), AM251 administration reduced the pHluorin signal
290 increase evoked by the 400 APs (ΔF_{400APs}) by 53.8 ± 17.0% in average (p < 0.001, by paired t-test),

291 with no change in its decay time course (τ_{decay}: 42.1 ± 7.8 to 40.9 ± 4.5 sec, p = 0.780, paired t-test)
292 (Figure 7C). The AP-triggered increase in pHluorin fluorescence was specific to axonal varicosities,
293 and the GPR55 activation reduced the size of the fluorescence increase with substantial variability
294 among individual boutons (Figure 7B-D). Altered abundance of GPR55 in distinct boutons might be
295 responsible for the variable effect of AM251 (see Figure 2). Interestingly, however, plotting the extent
296 of release reduction by AM251 against the original size of ΔF_{400APs} indicated that boutons showing a
297 larger amount of release tend to be more susceptible to suppression by the GPR55 activation (Figure
298 7E). This indicates that the variable control of the synaptic output exerted by GPR55 depends on the
299 original amount of release in individual boutons along a PC axon. On the other hand, when the
300 intracellular vesicles with an acidic internal lumen were ubiquitously neutralized by exogenous
301 application of NH_4Cl (50 mM), as depicted in Figure 7A, pHluorin fluorescence increased by 356.8 ±
302 12.3% in the control condition and 352.3 ± 14.0% in the presence of AM251 (p = 0.811, Student's t-
303 test) (Figure 7F, G), indicating that the total amount of vesicles at individual boutons is not affected
304 by GPR55 activation. It should be noted that ΔF_{400APs} by itself exhibited a large variability across
305 boutons, showing a linear relation to the 2/3rd power (for calibration between volume and surface
306 area of boutons) of that by NH_4Cl (ΔF_{NH4Cl}) (Figure 7H). Thus, the fraction of releasable vesicles in
307 response to APs seemed constant among distinct boutons: larger boutons containing more vesicles
308 simply show higher ΔF_{400APs}. In addition, the predicted distribution pattern of ΔF_{400APs} with GPR55
309 activation calculated from the relation between the extent of GPR55-mediated release reduction and
310 the ΔF_{400APs} (shown in Figure 7E) nicely overlapped the actual data obtained after the AM251
311 application (Figure 7H). Thus, the fluorescent live imaging of AP-triggered vesicle fusion revealed that
312 GPR55 reduces vesicular fusion in response to APs, without changing total vesicles present at
313 individual PC boutons.

314 To obtain further insights into the dynamics of synaptic vesicular pools possibly affected by
315 GPR55, such as transitions among the readily-releasable, recycling, reserve, and release-reluctant
316 pools at individual boutons (Fernandez-Alfonso and Ryan, 2008; Kim and Ryan, 2010; Cazares et al.,
317 2016; Mori et al., 2021), we repeatedly induced the 400 APs firing at the soma and measured the size
318 of the fluorescence increase at boutons before and after the suppression of re-acidification of
319 endocytosed vesicles with bafilomycin (100 nM), an inhibitor of vesicular ATPase (Sankaranarayanan
320 and Ryan, 2001). As shown in Figure 8A (black trace), bafilomycin application enhanced the ΔF_{400APs}
321 (by 55.9 ± 12.8%, p < 0.001, paired t-test), and abolished the fluorescence decay after the end of the
322 stimulation (relative ΔF_{400APs} remaining at 40 sec after the end of APs: 59.8 ± 18.6 (control) to 97.6 ±
323 4.6% (bafilomycin), p = 0.0261, paired t-test), reflecting the inhibition of the re-acidification of
324 endocytosed vesicles, which takes place in naïve conditions during and tens of seconds after the
325 stimulation. Repeating the 400 APs stimulations after the bafilomycin application resulted in additive
326 fluorescence increase, eventually reaching a plateau at 27.6 ± 2.6% of the maximal fluorescence

327 increase observed after the NH_4Cl application (Figure 8A). Imaging of presynaptic Ca^{2+} increase with
328 GCaMP7f expressed in PCs by AAV showed that Ca^{2+} increase upon 400 APs remained constant
329 during repetitive AP trains (Figure 8—figure supplement 1A, B). Thus, synaptic vesicles
330 corresponding to those for ~1000 APs are totally release-competent at individual axon terminals, in
331 accord with previous studies (Kawaguchi and Sakaba, 2015). In order to induce the exocytosis of the
332 remaining releasable vesicles in the terminal, if any, after the 8 sets of 400 APs train stimulation, KCl
333 (50 mM) was added to the external bath to potently depolarize the plasma membrane, resulting in
334 widespread elevation of intracellular Ca^{2+} (Figure 8—figure supplement 1). Nevertheless, little further
335 increase in the pHluorin signal was observed upon KCl application (Figure 8A), confirming that most
336 depolarization-sensitive vesicles have undergone fusion during the AP trains.

337 Intriguingly, the ΔF_{400APs} reduction by AM251 (red trace in Figure 8A) was evident throughout
338 the 400 APs train stimulations (~10 minutes in total), reaching a plateau of about 13.2 ± 1.4% of the
339 total amount of vesicles (Figure 8A, $p < 0.001$, compared with control (27.6 ± 2.6%), Student's t-test).
340 This implies that the total releasable vesicles upon repeated APs for minutes, which are composed
341 of the RRP, the recycling pool, and even some reserve pool of vesicles, get smaller in number when
342 GPR55 is activated. To further obtain insight into the reduced releasable vesicles by GPR55, we
343 triggered vesicular release from PC boutons by causing an aberrant cytoplasmic Ca^{2+} increase by
344 adding ionomycin, which forms Ca^{2+}-conducting pores on the plasma membrane. Indeed, when
345 monitored by GCaMP7f fluorescence imaging, ionomycin (10 μM) induced a much more potent and
346 broader Ca^{2+} increase throughout PC axons than the Ca^{2+} increase induced by the inflow through
347 VGCCs upon APs stimulation (Figures 8C-E and Figure 8—figure supplement 1C; $\Delta F/F$ upon 400
348 APs and ionomycin: varicosity, 5.3 ± 0.4 and 16.2 ± 0.9, $p < 0.001$, Tukey-Kramer test; axon, 1.6 ±
349 0.2 and 15.1 ± 1.0, $p < 0.001$, respectively). Consequently, surprisingly, application of ionomycin
350 increased pHluorin signal to almost identical levels irrespective of the GPR55 activation (54.0 ± 1.6%
351 and 58.1 ± 3.9% of total vesicles without and with AM251, respectively, $p = 0.356$, Student's t-test)
352 (Figure 8B). It should be noted that the size of the vesicle pool which underwent fusion upon the
353 ionomycin application was almost double of the pool which underwent exocytosis upon thousands of
354 APs. Thus, only a half population of Ca^{2+}-responsive releasable vesicles may be sensitive to APs in
355 naïve PC axonal terminals, which is further reduced when GPR55 is activated.
356
357
358 **Discussion**

359 In this study, we used a combination of subcellular patch-clamp recordings from axon
360 terminals and fluorescence imaging of presynaptic vesicular exocytosis in cerebellar primary cultures,
361 together with electrophysiology in cerebellar slices, and demonstrated that synaptic transmission from
362 PCs is suppressed by activation of GPR55, a type of cannabinoid receptor. The mechanism of action

363 involves a transformation of the presynaptic vesicles into insensitive to APs, while the Ca^{2+} influx is
364 kept constant in the terminal. Thus, a unique mechanism to negatively control synaptic outputs is
365 unveiled here, which would provide a way to fine-tune the neuronal computation in the brain in
366 coordination with the modulation of synaptic efficacy by conventional cannabinoid receptors.
367
368 **Modulation of synaptic function by endocannabinoids**
369 Following the findings of critical roles of CB1 receptor in fine tuning of neuronal circuit function,
370 another type of cannabinoid receptor, GPR55, was identified (Baker et al., 2006; Oka et al., 2007).
371 GPR55 seems to be activated by 2-AG and anandamide, similarly to CB1 or cannabinoid receptor
372 type 2 (CB2), although the downstream signaling is different, and also shows affinity to cannabidiol,
373 another molecule found in cannabis (Henstridge et al., 2008; Oka et al., 2009). Distinct from typical
374 chemical components of cannabis such as tetrahydrocannabinol (THC), cannabidiol has been shown
375 to modulate the function of nervous system with limited addictive power, and thus has attracted
376 attention for possible therapeutic applications to mental disorders (Denis et al., 2024). Thus, the
377 physiological actions of GPR55 are now increasingly studied, although its detailed effect on neuronal
378 computation still remains largely veiled. Here, we observed a remarkable suppression of presynaptic
379 function by GPR55 in PC boutons through a change in the releasable vesicle amounts and/or
380 properties. Pioneering studies clarified an important role of GPR55 in synaptic transmission at
381 hippocampal excitatory synapses, demonstrating presynaptic enhancement of glutamate release
382 presumably by elevating the cytoplasmic residual Ca^{2+} via release from intracellular stores (Sylantyev
383 et al., 2013; Rosenberg et al., 2023), in contrast to the suppression of release in our observation. The
384 lack of positive modulation of AP-triggered release through residual Ca^{2+} in PC terminals might be
385 due to abundant amount of potent Ca^{2+} buffer calbindin (Fierro and Llano, 1996). Indeed, increased
386 vesicular fusion only for the AP-insensitive spontaneous vesicular release (as mIPSCs) was observed
387 upon the IP_3-mediated Ca^{2+} release from internal store (Gomez et al., 2020). Thus, minimal sensitivity
388 of AP-triggered release to residual Ca^{2+} in PC boutons would underlie the distinct effects of GPR55
389 activation at the presynaptic side. In addition, Rosenberg et al. (2023) also demonstrated postsynaptic
390 modulation by GPR55 at hippocampal inhibitory synapses: reduction of postsynaptic $GABA_A$
391 receptors whereas limited presynaptic expression of GPR55 at axons. Here we showed clear GPR55
392 signals at PC terminals (see Figure 2), whereas no detectable changes in mIPSC amplitudes were
393 observed upon GPR55 activation in potential DCN neurons (see Figure 4E, F). Thus, distinct
394 combination of critical factors, such as amount and/or location of GPR55 expression, subtypes of
395 postsynaptic $GABA_A$ receptors, and/or their anchoring mechanism, might give rise to various forms of
396 modulation of synaptic strength by GPR55, as demonstrated in the hippocampus and cerebellum.
397 One extensively studied activity-dependent short-term depression of synaptic strength in the
398 CNS is DSE and/or DSI, which are typically caused by a strong postsynaptic depolarization
399 accompanied with potent Ca^{2+} increases or activation of G_q-coupled metabotropic receptors such as

400 group-I mGluRs, activating PLC and/or diacylglycerol lipase. Both enzymes produce typical
401 endocannabinoids such as 2-AG and anandamide, which then reach retrogradely presynaptic
402 boutons beyond plasma membranes and synaptic cleft (Kano et al., 2009; Castillo et al., 2012). As a
403 result, CB1 receptor located at the presynaptic membrane is activated and then Ca^{2+}-triggered
404 transmitter release is suppressed for tens of seconds (Kreitzer and Regehr, 2001; Ohno-Shosaku et
405 al., 2001; Wilson and Nicoll, 2001; Diana et al., 2002). Such short-term forms of presynaptic plasticity
406 have been found to take place at a variety of synapses in the CNS including the hippocampus,
407 cerebellum, prefrontal cortex, amygdala, and so on (Kano et al., 2009; Di Marzo et al., 2001; Katona
408 2001; Hill and Patel, 2013), which has provided basic knowledge about the primary mechanisms of
409 cannabis intake affecting brain computation. In addition, CB1 receptor has been shown to play roles
410 in long-term synaptic plasticity and hence learning and memory in animals (Kano et al., 2009; Gómez-
411 Gonzalo et al., 2015). On the other hand, the functional role of another cannabinoid receptor CB2 has
412 been largely unknown. CB2 receptor exogenously expressed in hippocampal autaptic neurons from
413 CB1 null mice was shown to suppress synaptic transmission and restore DSE (Atwood et al., 2012).
414 In contrast, in spite of CB2 being expressed in PCs (Ashton et al., 2006), no modulation of synaptic
415 outputs from PC axons has been demonstrated (Hirono and Yanagawa, 2021). Thus, as
416 demonstrated here, PC axon terminals might be equipped with a compensatory mechanism to control
417 outputs through GPR55 in place of CB2 receptor.
418
419 **Mechanisms for synaptic modulations by GPR55 distinct from CB1/CB2 receptors**
420 Unlike typical metabotropic receptors, here we have shown that GPR55 reduces vesicular
421 exocytosis by converting the Ca^{2+}-sensitive release-competent vesicles into reluctant ones upon AP
422 arrival, without changing the Ca^{2+} influx and vesicular Ca^{2+} responsiveness (see Figure 3-8). Rapid
423 replenishment and/or endocytosis of synaptic vesicles are known to depend on actin dynamics (Lee
424 et al., 2012; Miki et al., 2016), which might be related to the altered vesicular sensitivity to Ca^{2+} influx
425 through VGCCs after the GPR55 activation. In any case, the unique control of presynaptic function
426 by $G\alpha_{12/13}$-coupled GPR55 demonstrated here would provide a complementary modulation of synaptic
427 outputs by cannabinoids together with CB1/CB2 receptors. Previous studies have clarified the
428 molecular mechanisms by which CB1 receptor negatively modulates synaptic transmission. As well
429 as a typical inhibitory modulation by metabotropic receptors such as group-II metabotropic glutamate
430 receptors and $GABA_B$ receptors (Kew et al., 2001; Takahashi et al., 1998; Bowery et al., 2002), CB1
431 and CB2 receptors are thought to couple to $G_{i/o}$-type trimeric G-protein, negatively regulating the
432 activation and/or conductance of VGCCs (Guo and Ikeda, 2004). Taking it into consideration that the
433 vesicular exocytosis steeply depends on the local Ca^{2+} concentration around the Ca^{2+} sensor,
434 synaptotagmin (Schneggenburger and Neher, 2000), the reduction of Ca^{2+} influx is enough to explain
435 the suppression of transmitter release. Interestingly, when activated for minutes in cerebellar granule
436 cells, CB1 receptor was also shown to downregulate the release competence of vesicles through their

437 displacement from active zone (Ramírez-Franco et al., 2014), which is reminiscent of the GPR55-
438 mediated RRP reduction we presented in this study. It would be interesting to highlight the difference
439 in mechanisms how distinct G-protein cascades modulate the release machinery in the future study.
440

441 **Dynamics of synaptic vesicles among distinct functional pools**

442 Inspired by the GPR55-mediated marked decrease in RRP vesicles demonstrated here by the
443 presynaptic C_m measurement and biophysical analysis, we live-imaged vesicular fusion with synapto-
444 pHluorin to functionally dissect the altered pools of vesicles in PC terminals (see Figures 7, 8).
445 Surprisingly, the reduction of release upon GPR55 activation was only evident when the release was
446 triggered by APs, but undetectable in response to ionomycin, indicating that the apparent RRP
447 reduction would be highly related to the source of cytoplasmic Ca^{2+} increase. Taking into
448 consideration that the RRP reduction was also evident when the Ca^{2+} increase was triggered by much
449 stronger stimulation (50 ms direct presynaptic depolarization or extracellular KCl application), the
450 discrepancy between the effects of GPR55 on release by the presynaptic depolarization and the Ca^{2+}
451 ionophore could be reasonably ascribed to the relationship between release sites and Ca^{2+} sources.
452 Alternatively, slower kinetics and more prolonged duration, in addition to higher amplitude, of Ca^{2+}
453 elevation upon ionomycin might somehow have resulted in more efficient trigger of exocytosis.
454 Notably, our imaging experiments indicated that the total recycling pool of vesicles which underwent
455 exocytosis by thousands of APs during ~10 minutes corresponds to only ~25% of total vesicles, that
456 is, a half of Ca^{2+}-sensitive release-competent vesicles that could fuse upon aberrant Ca^{2+} increase
457 via the Ca^{2+}-conducting ionophore (see Figure 8A, B). Because of the extremely potent and rapid
458 Ca^{2+} buffering system in the cytoplasm of PCs due to the abundant expression of calbindin (Fierro
459 and Llano, 1996), the Ca^{2+} influx from VGCCs is expected to activate vesicles with the Ca^{2+} sensor
460 very close to the VGCCs. Thus, it is implied that the release-competent vesicles relatively far from
461 VGCCs tend to stay at their position for minutes without being exocytosed or getting into the AP-
462 sensitive pools. Indeed, it was shown that the relatively large increase in the cytoplasmic Ca^{2+}
463 concentration by IP_3-caused release from the internal Ca^{2+} store in PC terminals, is only effective for
464 the AP-independent spontaneous vesicular releases detected as miniature postsynaptic responses
465 (Gomez et al., 2020). Thus, at least in PCs, the functional categorization of depolarization-sensitive
466 vesicles seems to be influenced by the physical distance of vesicles and the source of Ca^{2+}.
467 Interestingly, the reduction of releasable vesicles by GPR55 activation is limited to the AP-sensitive
468 ones among Ca^{2+}-sensitive ones (see Figure 8). Taking the two findings together into consideration
469 that GPR55 suppresses more potently the release caused by smaller Ca^{2+} increase in the presence
470 of high EGTA (see Figure 5) and delays the onset of release (see Figure 6), it would be reasonable
471 to presume that the functional coupling between VGCCs and release machinery is loosened by the
472 GPR55 activation. The loosened Ca^{2+}-release coupling, if any, upon GPR55 activation operating as
473 the mechanism for synaptic suppression would compromise with the lack of changes in frequency of

474 mIPSCs (see Figure 4B, C). The fact that GPR55 activation leads to altered actin cytoskeleton
475 organization also makes this scenario plausible. Alternatively, it is also conceivable that GPR55 rather
476 decreases the Ca^{2+}-dependent vesicle replenishment (Hosoi et al., 2007), which possibly leads to
477 lower occupancy of release sites with release-competent vesicles, resulting in smaller total exocytic
478 events in response to long depolarization (like that for 50 ms). This scenario would compromise with
479 the tendency of more potent suppression of release by GPR55 with stronger Ca^{2+} buffering by higher
480 EGTA (see Figure 5D). On the other hand, it would also be possible that GPR55 somehow drives
481 immature vesicles to the release sites, such as those immediately after endocytosed from the plasma
482 membrane (Tran et al., 2023), leading to apparent reduction of transmitter release. Recent direct
483 patch-clamp recordings combined with super-resolution fluorescence or electron microscopic imaging
484 are highlighting the dynamic change of the Ca^{2+}-release coupling distance and/or efficacy (Fukaya et
485 al., 2021; Midorikawa et al., 2024). The exact change of release machinery relative to VGCCs at high
486 resolution of ~ nm in PC boutons upon GPR55 activation is a critical issue to be clarified in the future.
487
488 **Issues remain to be clarified in GPR55-mediated synaptic modulation**
489 There are important issues to be unveiled in the future, as clarified for CB1 receptor: what
490 neuronal situation leads to the production of endogenous GPR55 ligands like LPI, and how are the
491 synapses modulated in terms of strength and time course? Multiple isoforms of LPI are known to have
492 different chain length and unsaturation level, leading to distinct influence on GPR55 (Brenneman et
493 al., 2025). The soy-derived LPI (obtained from Merck #L7635) which we used in this study, contains
494 ~58% C16:0 and ~42% C18:0 or C18:2, and is known to exert neuroprotective and anti-inflammatory
495 effects in cultured DRG neurons (Brenneman et al., 2025), together with just a little of the C20:4
496 isoform promoting neuroinflammatory action. Intracellular Ca^{2+} elevation, such as pharmacologically
497 caused seizures, leads to the LPI production at various CNS regions including the hippocampus
498 (Yamashita et al., 2010; Rosenberg et al., 2023), although little is known about LPI in the cerebellum.
499 Expression of LPI-producing phospholipase A1 and A2 in PCs (Shirai and Ito, 2004) would be a clue
500 to study this issue.
501 In spite of the labeling of PC boutons with a fluorescent analogue of AM251 dependent on
502 GPR55 gene expression (see Figure 2), direct evidence of specific localization of GPR55 at PC
503 boutons, for example by immuno-labeling, is missing at present due to the unavailability of a qualified
504 and specific antibody as far as we have tested. Further, the present study could not identify the
505 downstream mechanism how GPR55 deprives the release competent vesicles of sensitivity to APs.
506 GPR55-coupled $G\alpha_{12/13}$–RhoA–actin pathway is expected to underlie, and detailed biophysical
507 analysis in the future would answer which of Ca^{2+}-release coupling or Ca^{2+}-dependent vesicle
508 replenishment is a likely candidate.
509
510

511 **Materials and Methods**

512 **Animal usage**

513 All experimental procedures were performed in accordance with regulations on animal
514 experimentation in Kyoto University and approved by the local committee in Graduate School of
515 Science, Kyoto University. Wistar rats (Slc: Wistar; Japan Slc Inc., Hamamatsu, Japan) of either sex
516 were used in this study. Rats were housed with a mother rat until weaning in filter-top cages with
517 bedding at 20−24°C under a 12/12 h light/dark photocycle. Food and water were available *ad libitum*.
518 Rats were killed by decapitation, and older ones by anaesthetization with isoflurane in air, then
519 decapitation.

520

521 **Slice preparation**

522 Acute sagittal slices (200 μm thickness) of cerebellum were prepared from Wistar rats at P28-42. Rats
523 were anesthetized with isoflurane and perfused transcardially with ice-cold sucrose solution
524 containing the following (in mM): NaCl 60, sucrose 120, $NaHCO_3$ 25, NaH_2PO_4 1.25, KCl 2.5, D-
525 glucose 25, ascorbic acid 0.4, myo-inositol 3, Na-pyruvate 2, $CaCl_2$ 0.1, $MgCl_2$ 3, pH 7.3-7.4, 300-350
526 mOsm/kg H_2O with continuous bubbling with mixed gas (95% O_2 and 5% CO_2). After decapitation,
527 the cerebellum was quickly removed and cut with a Leica vibroslicer (VT1200S) in an ice-cold K-
528 Gluconate-based solution containing the following (in mM): K-Gluconate 130, KCl 15, EGTA (ethylene
529 glycol-bis(β-aminoethyl ether)-N,N,N′,N′-tetraacetic acid) 0.05, HEPES (4-(2-hydroxyethyl)-1-
530 piperazineethanesulfonic acid) 20, glucose 25, and D-AP5 50 μM, pH 7.4, 300-350 mOsm/kg H_2O,
531 with continuous bubbling with mixed gas (95% O_2 and 5% CO_2). Slices were then incubated at 37 °C
532 for a half to 1 h in an extracellular solution containing the following (in mM): NaCl 125, $NaHCO_3$ 25,
533 NaH_2PO_4 1.25, KCl 2.5, D-glucose 25, ascorbic acid 0.4, myo-inositol 3, Na-pyruvate 2, $CaCl_2$ 2,
534 $MgCl_2$ 1, pH 7.3-7.4, 300-320 mOsm/kg H_2O with continuous bubbling with mixed gas.

535

536 **Cerebellar primary cultures**

537 The method for preparing primary dissociated cultures of cerebellar neurons was similar to that in
538 previous studies (Kawaguchi and Hirano, 2007). Briefly, cerebella were dissected out from newborn
539 rats and their meninges were removed. The cerebella were incubated in Ca^{2+} and Mg^{2+}-free Hank's
540 balanced salt solution containing 0.1% trypsin and 0.05% DNase for 15 min at 37°C. Cells were
541 dissociated by trituration and seeded in Dulbecco's modified Eagle's medium: nutrient mixture F12-
542 based medium containing 2% fetal bovine serum. On the next day, ~ 80% of medium was replaced
543 by basal medium Eagle. After that, half of the medium was changed every 3−4 days. Cytosine
544 arabinoside (4 μM) was added to the medium to inhibit proliferation of glial cells. PCs could be visually
545 identified by large cell bodies and thick dendrites. Experiments were performed >21 days after
546 preparation of the culture.

547

548 **DNA construction and transfection**

549 Plasmids containing coding DNA sequences of synapto-pHluorin, EGFP, Venus, and GCaMP7f were
550 the same as previous studies (Kawaguchi and Hirano, 2007; Kawaguchi and Sakaba, 2015; Higashi
551 et al., 2024). DNA fragments for tTA and TRE sequences were obtained from Tet-Off system
552 (Clontech). cDNAs were inserted into the pAAV-CA-WPRE plasmid (Higashi et al., 2024). PCs were
553 transfected with an AAV vector serotype 2 at 4-7 days after seeding. For GPR55-KD, the S. pyogenes
554 Cas9 vector plasmid, pSpCas9(BB)-2A-miRFP670 was obtained from Addgene (#91854). Two
555 gRNAs specific to GPR55 were designed with the CHOPCHOP online software. The target
556 sequences were designed to be separated by 81 base pairs so that the extracellular domain for
557 AM251 binding would be deleted (Joberty et al., 2020). The target sequences were cloned into the
558 plasmid based on the published protocol by Ran et al., 2013. Briefly, pSpCas9(BB)-2A-miRFP670
559 was digested with BbsI (New England Biolabs, USA) and the following oligos, 5'-
560 CACCGCCCCTGTGGAAAGTGTAGAT-3' and 5'-AAACATCTACACTTTCCACAGGGGC-3', or 5'-
561 CACCGTGCGAGAGTCTTCTTCCCCC-3' and 5'-AAACGGGGGAAGAAGACTCTCGCAC-3'
562 (Eurofins Genomics, Japan), were annealed and ligated into the digested plasmid. For GPR55-KD
563 using CRISPR/Cas9 or some imaging experiments using synapto-pHluorin, the DNA expression
564 plasmids encoding Cas9 and gRNAs, or synapto-pHluorin were directly injected into the nucleus of
565 PCs through sharp glass pipettes (Kawaguchi and Hirano, 2007). Recordings from DNA-injected cells
566 were performed 1–2 days after the injection, except for GPR55-KD cells with CRISPR/Cas9-mediated
567 acute genome editing (at 5 days).

568

569 **Electrophysiology**

570 Patch-clamp recording was performed with an amplifier (EPC10, HEKA Elektronik, Germany) at room
571 temperature (20-24 °C), in an extracellular solution mentioned above for slices, or that containing the
572 following for culture (in mM): NaCl 145, HEPES 10, glucose 10, $CaCl_2$ 2, $MgCl_2$ 1, pH 7.3-7.4 adjusted
573 with KOH, and 300-310 mOsm/kg H_2O, using an inverted IX71 microscope (Olympus, Tokyo, Japan)
574 equipped with a 40×, 0.95 numerical aperture (NA) objective or an upright BX51WI (Olympus)
575 equipped with a 60×, 1.0 NA objective. Images were obtained with a Zyla4.2 sCMOS camera (Andor;
576 Oxford Instruments, Oxford, UK). In some experiments, 2,3-Dioxo-6-nitro-1,2,3,4-
577 tetrahydrobenzo[f]quinoxaline-7-sulfonamide (NBQX, 10 μM), tetrodotoxin (TTX, 1 μM) and
578 tetraethylammonium (TEA, 2 mM) were applied to the bath. For current-clamp recordings, KCl-based
579 internal solution with the following composition (in mM) was used: KCl 147, HEPES 10, EGTA 0.5,
580 Mg-ATP 2, Na-GTP 0.2, pH 7.3-7.4 adjusted with KOH, and 320-330 mOsm/kg H_2O. For voltage-
581 clamp recordings from PC-target neurons, a patch pipette was filled with a CsCl-based internal
582 solution (pH 7.3-7.4 adjusted with CsOH and 320-330 mOsm/kg H_2O) containing (in mM): CsCl 147,
583 HEPES 10, EGTA 0.5, Mg-ATP 2, Na-GTP 0.2. For voltage-clamp recordings from PC axon terminals,

584 the internal solution was composed of (in mM): CsCl 103, KCl 44, HEPES 10, EGTA 0.5, Mg-ATP 2,
585 Na-GTP 0.2 (pH 7.3-7.4 adjusted with CsOH and 320-330 mOsm/kg H_2O). In a subset of experiments
586 shown in Figure 5, the EGTA concentration was increased to 5 mM. Presynaptic terminal recordings
587 were performed in the presence of external TTX (1 μM) and TEA (2 mM). AM251 (5 μM for slice or
588 500 nM for culture; EC_{50} = 39 nM, Ryberg et al., 2007), LPI (1 μM; EC_{50} = 30 nM, Oka et al., 2007),
589 or CID16020046 (5 μM; IC_{50} = 0.21 μM, Kargl et al., 2013) were applied to the bath. LPI derived from
590 soy (Merck, catalog #L7635) that was estimated to contain 58% C16:0 and 42% C18:0 or C18:2 was
591 applied to the bath. Membrane potential of a PC was held at -70 mV unless otherwise stated. PCs'
592 target postsynaptic neurons were voltage clamped at -70 to -100 mV (to avoid unclamped Na^+
593 currents) in slices, or at -70 mV in culture for IPSC recordings. Series resistance in recordings from
594 the PC soma and axon terminal was online-compensated by 30−60%. For IPSC measurements, the
595 remaining resistance was corrected off-line after the recording. In paired whole-cell recordings from
596 a presynaptic PC soma and its postsynaptic neuron, APs were elicited by voltage pulses to 0 mV for
597 1-5 ms into PC soma. In the slice, IPSCs were evoked by a glass pipette placed in the white matter.
598 The deconvolution analysis was performed as in a previous study (Kawaguchi and Sakaba, 2015)
599 using a template of mIPSC waveform. The onset of release was defined as the first time point at which
600 the calculated vesicular fusion velocity showed change larger than 2 SDs of that at the basal condition.
601 Average amplitude and frequency of mIPSCs for individual cells were calculated from ≥ 200 events
602 showing amplitude (≥ 7 pA) and appropriate time course.
603 Measurement of C_m was done using sine + DC technique (Neher and Marty, 1982)
604 implemented on the PatchMaster software (HEKA Elektronik, Germany). Presynaptic terminals were
605 held at -80 mV and the sine wave (1 kHz and the peak amplitude of 30 mV) was applied on the holding
606 potential. Because membrane conductance fluctuates during the depolarizing pulse, C_m was usually
607 measured approximately 50 ms after the depolarization. To estimate the clamped area in a direct
608 bouton recording, capacitive transients in response to a hyperpolarizing pulse (5 or 10 mV) were used.
609 To normalize the variation in Ca^{2+} currents and neurotransmitter release depending on the size of the
610 bouton, presynaptic Ca^{2+} current and C_m were normalized by the C_m under the voltage-clamp in each
611 bouton (in Figure 3-6).
612
613 **Fluorescence imaging**
614 For GPR55 fluorescent labeling, cultured neurons were incubated with T1117 (20 nM) in extracellular
615 solution for 2 min at room temperature. Following incubation, cells were washed once with fresh
616 extracellular solution to remove unbound dye and immediately imaged with a confocal fluorescence
617 imaging system FV1000 (Olympus) using a 60× 0.9-NA water-immersion objective (Olympus)
618 equipped on an upright microscope BX61WI. Fluorescence imaging of pHluorin or GCaMP7f was
619 performed using an upright microscope BX51WI (Olympus) through a 60× 1.0-NA objective

620 (Olympus). Fluorescent excitation was delivered using an LED (M470L4, Thorlabs). Images of
621 pHluorin or GCaMP7f fluorescence in PC axon terminals were obtained at 0.5 Hz with Zyla4.2 sCMOS
622 camera (Andor), and analyzed with SOLIS (Andor) or ImageJ (NIH). APs were evoked at the voltage-
623 clamped PC soma by depolarizing pulses (0 mV, 5 ms). Bafilomycin (100 nM), ionomycin (10 μM),
624 KCl (50 mM), and NH_4Cl (50 mM) were applied to the bath.
625
626 **Statistics**
627 Data are presented as mean ± SEM unless otherwise stated. Statistical significance was evaluated
628 by paired t-test, unpaired Student's t-test for unpaired groups, one-way ANOVA, Dunnett's test or
629 Tukey-Kramer test for multiple comparisons. Statistical significance was defined as $p < 0.05$.
630
631
632 **Acknowledgments**
633 We thank Drs. Mitsuharu Midorikawa and Federico Trigo for the critical reading of the manuscript and
634 helpful comments.
635
636
637 **Competing interests**
638 The authors declare no competing interests.
639
640
641 **Funding**
642 Japan Society for the Promotion of Science, KAKENHI grants 25K02362 (SK), 25H02611 (SK),
643 22H02721 (SK), 22K19360 (SK), 24K18217 (TI) and 21K15189 (TI). Takeda Science Foundation
644 (SK). Naito Foundation (SK).

References

1. Abbott LF, Regehr WG. (2004) **Synaptic computation** *Nature* **431**:796-803. DOI: https://doi.org/10.1038/nature03010, PMID: 15483601
2. Adler EM, Augustine GJ, Duffy SN, Charlton MP. (1991) **Alien intracellular calcium chelators attenuate neurotransmitter release at the squid giant synapse** *The Journal of Neuroscience* **11**:1496–1507. DOI: https://doi.org/10.1523/JNEUROSCI.11-06-01496.1991, PMID: 1675264
3. Ashton JC, Friberg D, Darlington CL, Smith PF. (2006) **Expression of the cannabinoid CB2 receptor in the rat cerebellum: an immunohistochemical study** *Neuroscience Letters* **396**:113-116. DOI: https://doi.org/10.1016/j.neulet.2005.11.038, PMID: 16356641
4. Atwood BK, Straiker A, MacKie K. (2012) **CB_2 cannabinoid receptors inhibit synaptic transmission when expressed in cultured autaptic neurons** *Neuropharmacology* **63**:514–523. DOI: https://doi.org/10.1016/j.neuropharm.2012.04.024, PMID: 22579668
5. Baker D, Pryce G, Davies WL, Hiley CR. (2006) **In silico patent searching reveals a new cannabinoid receptor** *Trends in Pharmacological Sciences* **27**:1–4. DOI: https://doi.org/10.1016/j.tips.2005.11.003, PMID: 16318877
6. Bornschein G, Arendt O, Hallermann S, Brachtendorf S, Eilers J, Schmidt H. (2013) **Paired-pulse facilitation at recurrent Purkinje neuron synapses is independent of calbindin and parvalbumin during high-frequency activation** *The Journal of Physiology* **591**:3355-3370. DOI: https://doi.org/10.1113/jphysiol.2013.254128, PMID: 23671160
7. Borst JG, Sakmann B. (1996) **Calcium influx and transmitter release in a fast CNS synapse** *Nature* **383**:431–434. DOI: https://doi.org/10.1038/383431a0, PMID: 8837774
8. Bowery NG, Bettler B, Froestl W, Gallagher JP, Marshall F, Raiteri M, Bonner TI, Enna SJ. (2002) **International Union of Pharmacology. XXXIII. Mammalian gamma-aminobutyric acid(B) receptors: structure and function** *Pharmacological Reviews* **54**:247-264. DOI: https://doi.org/10.1124/pr.54.2.247, PMID: 12037141
9. Brenneman DE, Petkanas D, Ippolito M, Ward SJ. (2025) **Effect of Fatty Acyl Composition for Lysophosphatidylinositol on Neuroinflammatory Responses in Primary Neuronal Cultures** *Journal of Molecular Neuroscience* **75**:35. DOI: https://doi.org/10.1007/s12031-025-02326-7, PMID: 40085305
10. Castillo PE, Younts TJ, Chávez AE, Hashimotodani Y. (2012) **Endocannabinoid signaling and synaptic function** *Neuron* **76**:70-81. DOI: https://doi.org/10.1016/j.neuron.2012.09.020, PMID: 23040807
11. Cazares VA, Njus MM, Manly A, Saldate JJ, Subramani A, Ben-Simon Y, Sutton MA, Ashery U, Stuenkel EL. (2016) **Dynamic Partitioning of Synaptic Vesicle Pools by the SNARE-Binding Protein Tomosyn** *The Journal of Neuroscience* **36**:11208-11222. DOI: https://doi.org/10.1523/JNEUROSCI.1297-16.2016, PMID: 27807164
12. Daly CJ, Ross RA, Whyte J, Henstridge CM, Irving AJ, McGrath JC. (2010) **Fluorescent ligand binding reveals heterogeneous distribution of adrenoceptors and 'cannabinoid-like' receptors in small arteries** *British Journal of Pharmacology* **159**:787-796. DOI: https://doi.org/10.1111/j.1476-5381.2009.00608.x, PMID: 20136833
13. Denis Völker JS, Micluția IV, Vinași RC. (2024) **Investigating Cannabidiol's potential as a supplementary treatment for schizophrenia: A narrative review** *European Journal of Pharmacology* **979**:176821. DOI: 10.1016/j.ejphar.2024.176821, PMID: 39068976
14. Devinsky O, Jones NA, Cunningham MO, Jayasekera BAP, Devore S, Whalley BJ. (2024) **Cannabinoid treatments in epilepsy and seizure disorders** *Physiological Reviews* **104**:591-649. DOI: https://doi.org/10.1152/physrev.00049.2021, PMID: 37882730
15. Di Marzo V, Goparaju SK, Wang L, Liu J, Bátkai S, Járai Z, Fezza F, Miura GI, Palmiter RD, Sugiura T, Kunos G. (2001) **Leptin-regulated endocannabinoids are involved in maintaining food intake** *Nature* **410**:822-825. DOI: https://doi.org/10.1038/35071088, PMID: 11298451
16. Diana MA, Levenes C, Mackie K, Marty A. (2002) **Short-term retrograde inhibition of GABAergic synaptic currents in rat Purkinje cells is mediated by endogenous cannabinoids** *The Journal of Neuroscience* **22**:200-208. DOI: https://doi.org/10.1523/JNEUROSCI.22-01-00200.2002, PMID: 11756503
17. Díaz-Rojas F, Sakaba T, Kawaguchi SY. (2015) **Ca^{2+} current facilitation determines short-term facilitation at inhibitory synapses between cerebellar Purkinje cells** *The Journal of Physiology* **593**:4889–4904. DOI: https://doi.org/10.1113/JP270704, PMID: 26337248

18. Fernandez-Alfonso T, Ryan TA. (2008) **A heterogeneous "resting" pool of synaptic vesicles that is dynamically interchanged across boutons in mammalian CNS synapses** *Brain Cell Biology* **36**:87-100. DOI: https://doi.org/10.1007/s11068-008-9030-y, PMID: 18941900
19. Fierro L, Llano I. (1996) **High endogenous calcium buffering in Purkinje cells from rat cerebellar slices** *The Journal of Physiology* **496**:617-625. DOI: https://doi.org/10.1113/jphysiol.1996.sp021713, PMID: 8930830
20. Fukaya R, Maglione M, Sigrist SJ, Sakaba T. (2021) **Rapid Ca^{2+} channel accumulation contributes to cAMP-mediated increase in transmission at hippocampal mossy fiber synapses** *PNAS* **118**:e2016754118. DOI: 10.1073/pnas.2016754118, PMID: 33622791
21. Furukawa K, Inoshita T, Kawaguchi SY. (2024) **Graded control of Purkinje cell outputs by cAMP through opposing actions on axonal action potential and transmitter release** *The Journal of Physiology* DOI: https://doi.org/10.1113/JP286668, PMID: 39052311
22. Gómez-Gonzalo M, Navarrete M, Perea G, Covelo A, Martín-Fernández M, Shigemoto R, Luján R, Araque A. (2015) **Endocannabinoids Induce Lateral Long-Term Potentiation of Transmitter Release by Stimulation of Gliotransmission** *Cerebral Cortex* **25**:3699-3712. DOI: https://doi.org/10.1093/cercor/bhu231, PMID: 25260706
23. Gomez LC, Kawaguchi SY, Collin T, Jalil A, Gomez MDP, Nasi E, Marty A, Llano I. (2020) **Influence of spatially segregated IP3-producing pathways on spike generation and transmitter release in Purkinje cell axons** *PNAS* **117**:11097-11108. DOI: https://doi.org/10.1073/pnas.2000148117, PMID: 32358199
24. Guo J, Ikeda SR. (2004) **Endocannabinoids modulate N-type calcium channels and G-protein-coupled inwardly rectifying potassium channels via CB1 cannabinoid receptors heterologously expressed in mammalian neurons** *Molecular Pharmacology* **65**:665-674. DOI: https://doi.org/10.1124/mol.65.3.665, PMID: 14978245
25. Harada K, Kitaguchi T, Kamiya T, Aung KH, Nakamura K, Ohta K, Tsuboi T. (2017) **Lysophosphatidylinositol-induced activation of the cation channel TRPV2 triggers glucagon-like peptide-1 secretion in enteroendocrine L cells** *The Journal of Biochemistry* **292**:10855-10864. DOI: https://doi.org/10.1074/jbc.M117.788653, PMID: 28533434
26. Henstridge CM, Balenga NA, Ford LA, Ross RA, Waldhoer M, Irving AJ. (2008) **The GPR55 ligand L-alpha-lysophosphatidylinositol promotes RhoA-dependent Ca^{2+} signaling and NFAT activation** *The FASEB Journal* **23**:183-193. DOI: https://doi.org/10.1096/fj.08-108670, PMID: 18757503
27. Higashi R, Morita M, Kawaguchi SY. (2024) **Cl^--dependent amplification of excitatory synaptic potentials at distal dendrites revealed by voltage imaging** *Science Advances* **10**:eadj2547. DOI: https://doi.org/10.1126/sciadv.adj2547, PMID: 39196927
28. Hill MN, Patel S. (2013) **Translational evidence for the involvement of the endocannabinoid system in stress-related psychiatric illnesses** *Biology of Mood & Anxiety Disorders* **3**:19. DOI: https://doi.org/10.1186/2045-5380-3-19, PMID: 24286185
29. Hirono M, Yanagawa Y. (2021) **Endocannabinoids regulate cerebellar GABAergic transmission in a synapse type-dependent manner** *Journal of Neuroscience Research* **99**:898–913. DOI: https://doi.org/10.1002/jnr.24765, PMID: 33271631
30. Hosoi N, Sakaba T, Neher E. (2007) **Quantitative analysis of calcium-dependent vesicle recruitment and its functional role at the calyx of Held synapse** *The Journal of Neuroscience* **27**:14286-14298. DOI: https://doi.org/10.1523/JNEUROSCI.4122-07.2007, PMID: 18160636
31. Joberty G, Fälth-Savitski M, Paulmann M, Bösche M, Doce C, Cheng AT, Drewes G, Grandi P. (2020) **A Tandem Guide RNA-Based Strategy for Efficient CRISPR Gene Editing of Cell Populations with Low Heterogeneity of Edited Alleles**. *The CRISPR Journal* **3**:123-134. DOI: https://10.1089/crispr.2019.0064, PMID: 32315231
32. Kandel ER. (2001) **The molecular biology of memory storage: a dialogue between genes and synapses** *Science* **294**:1030-1038. DOI: https://doi.org/10.1126/science.1067020, PMID: 11691980
33. Kano M, Ohno-Shosaku T, Hashimotodani Y, Uchigashima M, Watanabe M. (2009) **Endocannabinoid-mediated control of synaptic transmission** *Physiological Reviews* **89**:309-380. DOI: https://doi.org/10.1152/physrev.00019.2008, PMID: 19126760
34. Kargl J, Brown AJ, Andersen L, Dorn G, Schicho R, Waldhoer M, Heinemann A. (2013) **A selective antagonist reveals a potential role of G protein-coupled receptor 55 in platelet and endothelial cell function** *Journal of Pharmacology and Experimental Therapeutics* **346**:54-

759 66 DOI: https://doi.org/10.1124/jpet.113.204180, PMID: 23639801
760 35. Katona I, Rancz EA, Acsady L, Ledent C, Mackie K, Hajos N, Freund TF. (2001) **Distribution of**
761 **CB1 cannabinoid receptors in the amygdala and their role in the control of GABAergic**
762 **transmission** *The Journal of Neuroscience* **21**:9506-9518. DOI:
763 https://doi.org/10.1523/JNEUROSCI.21-23-09506.2001, PMID: 11717385
764 36. Kawaguchi SY, Hirano T. (2007) **Sustained structural change of GABA(A) receptor-**
765 **associated protein underlies long-term potentiation at inhibitory synapses on a cerebellar**
766 **Purkinje neuron** *Journal of Neuroscience Research* **27**:6788-99. DOI:
767 https://doi.org/10.1523/JNEUROSCI.1981-07.2007, PMID: 17581966
768 37. Kawaguchi SY, Sakaba T. (2015) **Control of inhibitory synaptic outputs by low excitability**
769 **of axon terminals revealed by direct recording** *Neuron* **85**:1273–1288. DOI:
770 https://doi.org/10.1016/j.neuron.2015.02.013, PMID: 25728570
771 38. Kew JN, Ducarre JM, Pflimlin MC, Mutel V, Kemp JA. (2001) **Activity-dependent presynaptic**
772 **autoinhibition by group II metabotropic glutamate receptors at the perforant path inputs to**
773 **the dentate gyrus and CA1** *Neuropharmacology* 40:20-27. DOI: https://doi.org/10.1016/s0028-
774 3908(00)00118-0, PMID: 11077067
775 39. Khan AA, Shekh-Ahmad T, Khalil A, Walker MC, Ali AB. (2018) **Cannabidiol exerts**
776 **antiepileptic effects by restoring hippocampal interneuron functions in a temporal lobe**
777 **epilepsy model** *British Journal of Pharmacology* **175**:2097–2115. DOI:
778 https://doi.org/10.1111/bph.14202, PMID: 29574880
779 40. Kim SH, Ryan TA. (2010) **CDK5 serves as a major control point in neurotransmitter release**
780 *Neuron* **67**:797-809. DOI: https://doi.org/10.1016/j.neuron.2010.08.003, PMID: 20826311
781 41. Kreitzer AC, Regehr WG. (2001) **Retrograde inhibition of presynaptic calcium influx by**
782 **endogenous cannabinoids at excitatory synapses onto Purkinje cells** *Neuron* **29**:717–727.
783 DOI: https://doi.org/10.1016/s0896-6273(01)00246-x, PMID: 11301030
784 42. Kushmerick C, Price GD, Taschenberger H, Puente N, Renden R, Wadiche JI, Duvoisin RM,
785 Grandes P, von Gersdorff H. (2004) **Retroinhibition of Presynaptic Ca^{2+} Currents by**
786 **Endocannabinoids Released via Postsynaptic mGluR Activation at a Calyx Synapse** *The*
787 *Journal of Neuroscience* **24**:5955. DOI: https://doi.org/10.1523/JNEUROSCI.0768-04.2004,
788 PMID: 15229243
789 43. Lee JS, Ho WK, Lee SH. (2012) **Actin-dependent rapid recruitment of reluctant synaptic**
790 **vesicles into a fast-releasing vesicle pool** *PNAS* **109**:765-774. DOI:
791 https://doi.org/10.1073/pnas.1114072109, PMID: 22393020
792 44. Mori Y, Takenaka KI, Fukazawa Y, Takamori S. (2021) **The endosomal Q-SNARE, Syntaxin 7,**
793 **defines a rapidly replenishing synaptic vesicle recycling pool in hippocampal neurons**
794 *Communications Biology* **4**:981. DOI: https://doi.org/10.1038/s42003-021-02512-4, PMID:
795 34408265
796 45. Midorikawa M, Sakamoto H, Nakamura Y, Hirose K, Miyata M. (2024) **Developmental**
797 **refinement of the active zone nanotopography and axon wiring at the somatosensory**
798 **thalamus** *Cell Reports* **43**:114770. DOI: https://doi.org/10.1016/j.celrep.2024.114770, PMID:
799 39321021
800 46. Miki T, Malagon G, Pulido C, Llano I, Neher E, Marty A. (2016) **Actin- and Myosin-Dependent**
801 **Vesicle Loading of Presynaptic Docking Sites Prior to Exocytosis** *Neuron* **91**:808-823. DOI:
802 https://doi.org/10.1016/j.neuron.2016.07.033, PMID: 27537485
803 47. Neher E, Marty A. (1982) **Discrete changes of cell membrane capacitance observed under**
804 **conditions of enhanced secretion in bovine adrenal chromaffin cells** *PNAS* **79**:6712–6716.
805 DOI: https://doi.org/10.1073/pnas.79.21.6712, PMID: 6959149
806 48. Neher E, Sakaba T. (2001) **Combining deconvolution and noise analysis for the estimation**
807 **of transmitter release rates at the calyx of held** *Journal of Neuroscience* **21**:444-461. DOI:
808 https://doi.org/10.1523/JNEUROSCI.21-02-00444.2001, PMID: 11160425
809 49. Nicholson-Tomishima K, Ryan TA. (2004) **Kinetic efficiency of endocytosis at mammalian**
810 **CNS synapses requires synaptotagmin I** *PNAS* **101**:16648-16652. DOI:
811 https://doi.org/10.1073/pnas.0406968101, PMID: 15492212
812 50. Ohno-Shosaku T, Maejima T, Kano M. (2001) **Endogenous cannabinoids mediate retrograde**
813 **signals from depolarized postsynaptic neurons to presynaptic terminals** *Neuron* **29**:729–
814 738. DOI: https://doi.org/10.1016/s0896-6273(01)00247-1, PMID: 11301031
815 51. Oka S, Nakajima K, Yamashita A, Kishimoto S, Sugiura T. (2007) **Identification of GPR55 as a**

lysophosphatidylinositol receptor *Biochemical and Biophysical Research Communications* **362**:928-934. DOI: https://doi.org/10.1016/j.bbrc.2007.08.078, PMID: 17765871

52. Oka S, Toshida T, Maruyama K, Nakajima K, Yamashita A, Sugiura T. (2009) **2-Arachidonoyl-sn-glycero-3-phosphoinositol: a possible natural ligand for GPR55** *The Journal of Biochemistry* **145**:13-20. DOI: https://doi.org/10.1093/jb/mvn136, PMID: 18845565
53. Ramírez-Franco J, Bartolomé-Martín D, Alonso B, Torres M, Sánchez-Prieto J. (2014) **Cannabinoid type 1 receptors transiently silence glutamatergic nerve terminals of cultured cerebellar granule cells** *PLoS One* **9**:e88594. DOI: https://doi.org/10.1371/journal.pone.0088594, PMID: 24533119
54. Ran FA, Hsu PD, Wright J, Agarwala V, Scott DA, Zhang F. (2013) **Genome engineering using the CRISPR-Cas9 system** *Natureprotocols* **8**:2281-2308. DOI: https://doi.org/10.1038/nprot.2013.143, PMID: 24157548
55. Rosenberg EC, Chamberland S, Bazelot M, Nebet ER, Wang X, McKenzie S, Jain S, Greenhill S, Wilson M, Marley N, Salah A, Bailey S, Patra PH, Rose R, Chenouard N, Sun SD, Jones D, Buzsáki G, Devinsky O, Woodhall G, Scharfman HE, Whalley BJ, Tsien RW. (2023) **Cannabidiol modulates excitatory-inhibitory ratio to counter hippocampal hyperactivity** *Neuron* **111**:1282-1300.e8. DOI: https://doi.org/10.1016/j.neuron.2023.01.018, PMID: 36787750
56. Ryberg E, Larsson N, Sjögren S, Hjorth S, Hermansson NO, Leonova J, Elebring T, Nilsson K, Drmota T, Greasley PJ. (2007) **The orphan receptor GPR55 is a novel cannabinoid receptor** *British Journal of Pharmacology* **152**:1092-1101. DOI: https://doi.org/10.1038/sj.bjp.0707460, PMID: 17876302
57. Sakaba T. (2006) **Roles of the fast-releasing and the slowly releasing vesicles in synaptic transmission at the calyx of Held** *The Journal of Neuroscience* **26**:5863-5871. DOI: https://doi.org/10.1523/JNEUROSCI.0182-06.2006, PMID: 16738227
58. Sankaranarayanan S, Ryan TA. (2000) **Real-time measurements of vesicle-SNARE recycling in synapses of the central nervous system** *Nature Cell Biology* **2**:197-204. DOI: https://doi.org/10.1038/35008615, PMID: 10783237
59. Sankaranarayanan S, Ryan TA. (2001) **Calcium accelerates endocytosis of vSNAREs at hippocampal synapses** *Nature Neuroscience* **4**:129-36. DOI: https://doi.org/10.1038/83949, PMID: 11175872
60. Schneggenburger R, Neher E. (2000) **Intracellular calcium dependence of transmitter release rates at a fast central synapse** *Nature* **406**:889-893. DOI: https://doi.org/10.1038/35022702, PMID: 10972290
61. Shallcross J, Hámor P, Bechard AR, Romano M, Knackstedt L, Schwendt M. (2019) **The Divergent Effects of CDPPB and Cannabidiol on Fear Extinction and Anxiety in a Predator Scent Stress Model of PTSD in Rats** *Frontiers in Behavioral Neuroscience* **13**:91. DOI: https://doi.org/10.3389/fnbeh.2019.00091, PMID: 31133832
62. Shirai Y, Ito M. (2004) **Specific differential expression of phospholipase A2 subtypes in rat cerebellum** *Journal of Neurocytology* **33**:297-307. DOI: https://doi.org/10.1023/B:NEUR.0000044191.83858.f7, PMID: 15475685
63. Sylantyev S, Jensen TP, Ross RA, Rusakov DA. (2013) **Cannabinoid- and lysophosphatidylinositol-sensitive receptor GPR55 boosts neurotransmitter release at central synapses** *PNAS* **110**:5193-5198. DOI: https://doi.org/10.1073/pnas.1211204110, PMID: 23472002
64. Takahashi T, Kajikawa Y, Tsujimoto T. (1998) **G-Protein-coupled modulation of presynaptic calcium currents and transmitter release by a GABAB receptor** *The Journal of Neuroscience* **18**:3138-3146. DOI: https://doi.org/10.1523/JNEUROSCI.18-09-03138.1998, PMID: 9547222
65. Tran V, Silva M, Marty A. (2023) **Prioritized docking of synaptic vesicles provided by a rapid recycling pathway** *iScience* **26**:106366. DOI: https://doi.org/10.1016/j.isci.2023.106366, PMID: 37009220
66. Tsou K, Brown S, Sañudo-Peña MC, Mackie K, Walker JM. (1998) **Immunohistochemical distribution of cannabinoid CB1 receptors in the rat central nervous system** *Neuroscience* **83**:393-411. DOI: https://10.1016/s0306-4522(97)00436-3, PMID: 9460749
67. Uusisaari M, Obata K, Knöpfel T. (2006) **Morphological and electrophysiological properties of GABAergic and non-GABAergic cells in the deep cerebellar nuclei** *Journal of Neurophysiology* **97**:901-911. DOI: https://doi.org/10.1152/jn.00974.2006, PMID: 17093116
68. Vyleta NP, Jonas P. (2014) **Loose coupling between Ca^{2+} channels and release sensors at a**

plastic hippocampal synapse *Science* **343**:665-670. DOI: https://doi.org/10.1126/science.1244811, PMID: 24503854

69. Weisskopf MG, Castillo PE, Zalutsky RA, Nicoll RA. (1994) **Mediation of hippocampal mossy fiber long-term potentiation by cyclic AMP** *Science* **265**:1878–1882. DOI: https://doi.org/10.1126/science.7916482, PMID: 7916482
70. Wilson RI, Nicoll RA. (2001) **Endogenous cannabinoids mediate retrograde signalling at hippocampal synapses** *Nature* **410**:588–592. DOI: https://doi.org/10.1038/35069076, PMID: 11279497
71. Wu CS, Chen H, Sun H, Zhu J, Jew CP, Wager-Miller J, Straiker A, Spencer C, Bradshaw H, Mackie K, Lu HC. (2013) **GPR55, a G-protein coupled receptor for lysophosphatidylinositol, plays a role in motor coordination** *PLoS One* **8**:e60314. DOI: https://doi.org/10.1371/journal.pone.0060314, PMID: 23565223
72. Wu Y, Liu Q, Guo B, Ye F, Ge J, Xue L. (2020) **BDNF Activates Postsynaptic TrkB Receptors to Induce Endocannabinoid Release and Inhibit Presynaptic Calcium Influx at a Calyx-Type Synapse** *The Journal of Neuroscience* **40**:8070-8087. DOI: https://doi.org/10.1523/JNEUROSCI.2838-19.2020, PMID: 3294867
73. Xia R, Yuan Q, Wang N, Hou L, Abe J, Song J, Ito Y, Xu HE, He Y. (2025) **Structural insight into GPR55 ligand recognition and G-protein coupling** *Cell Research* **35**:76-79. DOI: https://doi.org/10.1038/s41422-024-01044-w, PMID: 39482404
74. Yamashita M, Kawaguchi SY, Hori T, Takahashi T. (2018) **Vesicular GABA Uptake Can Be Rate Limiting for Recovery of IPSCs from Synaptic Depression** *Cell Rep*orts. **22**:3134-3141. DOI: https://doi.org/10.1016/j.celrep.2018.02.080, PMID: 29562170
75. Yamashita A, Kumazawa T, Koga H, Suzuki N, Oka S, Sugiura T. (2010) **Generation of lysophosphatidylinositol by DDHD domain containing 1 (DDHD1): Possible involvement of phospholipase D/phosphatidic acid in the activation of DDHD1** *Molecular and Cell Biology of Lipids* **1801**:711-720. DOI: https://doi.org/10.1016/j.bbalip.2010.03.012, PMID: 20359546
76. Zorrilla de San Martin J, Trigo FF, Kawaguchi SY. (2017) **Axonal GABAA receptors depolarize presynaptic terminals and facilitate transmitter release in cerebellar Purkinje cells** *The Journal of Physiology* **595**:7477-7493. DOI: https://doi.org/10.1113/JP275369, PMID: 29072780

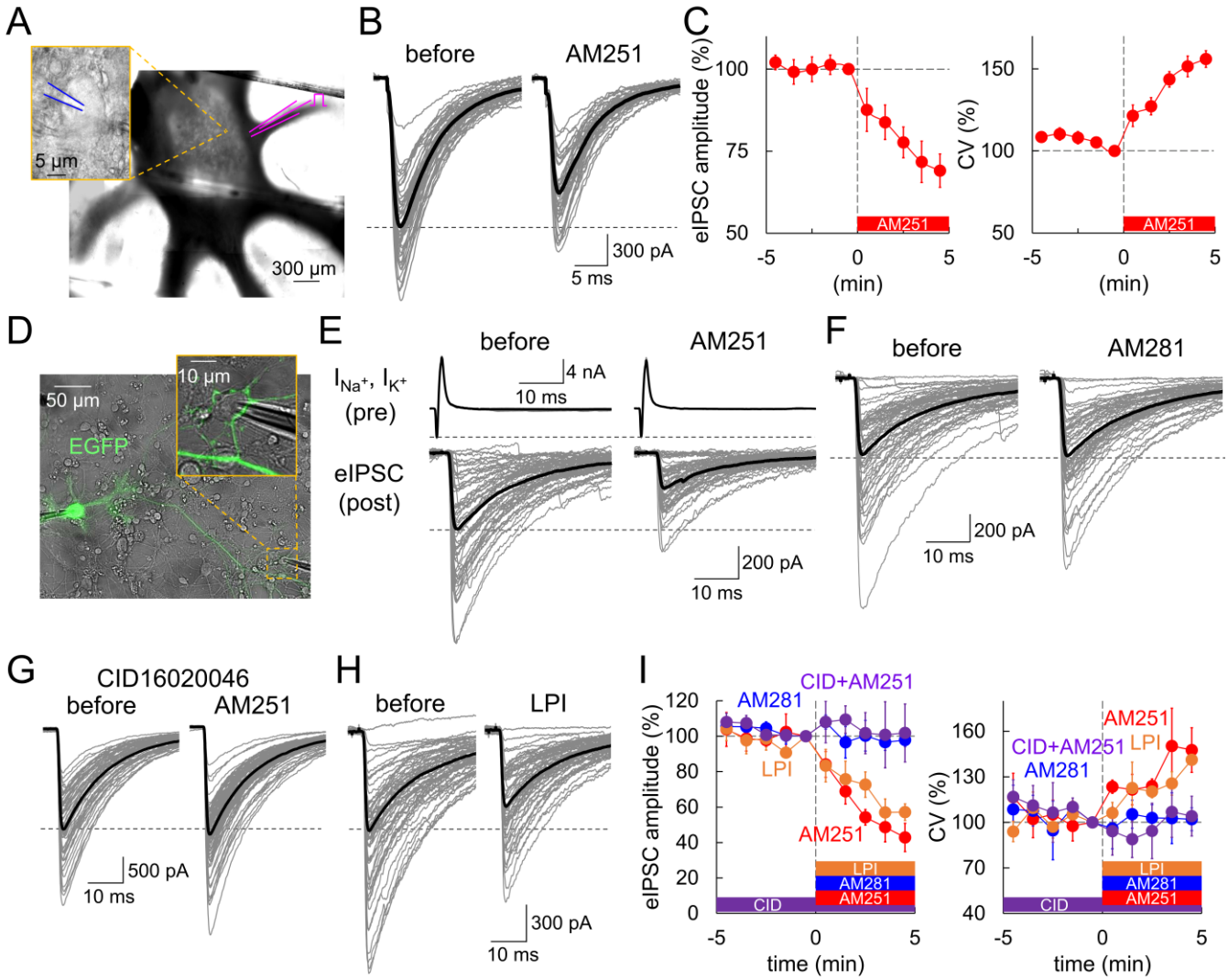

Figure 1. Reduced transmission at PC-DCN synapses by GPR55 in slice and culture
(**A**) Image of patch-clamp recording from a DCN neuron in slice. A magnified image of the recorded neuron is shown as an inset (a patch pipette is indicated in blue). A pipette for electrical stimulation (magenta) was placed at the white matter. (**B, C**) Individual (gray) and averaged (black) traces (B), and time courses of eIPSC amplitude (C, left) and CV (C, right) before and after the AM251 application (at time 0), n = 6. (**D**) Image of dual whole-cell recordings from a presynaptic EGFP-labeled PC soma and its postsynaptic target neuron in culture. (**E-H**) Representative traces of eIPSCs before and 5 minutes after the application of AM251 (E), AM281 (F), AM251 in the presence of CID (G), or LPI (H). In E, presynaptic Na^+ and the following K^+ currents (I_{Na^+}, I_{K^+}) at a presynaptic PC soma are also shown. (**I**) Time courses of eIPSC amplitude and CV. n = 6 (AM251), 5 (AM281), 5 (CID + AM251) and 5 cells (LPI). CID was applied from the beginning of the recording. The internal solution contained 0.5 mM EGTA. Data are shown as mean ± SEM.

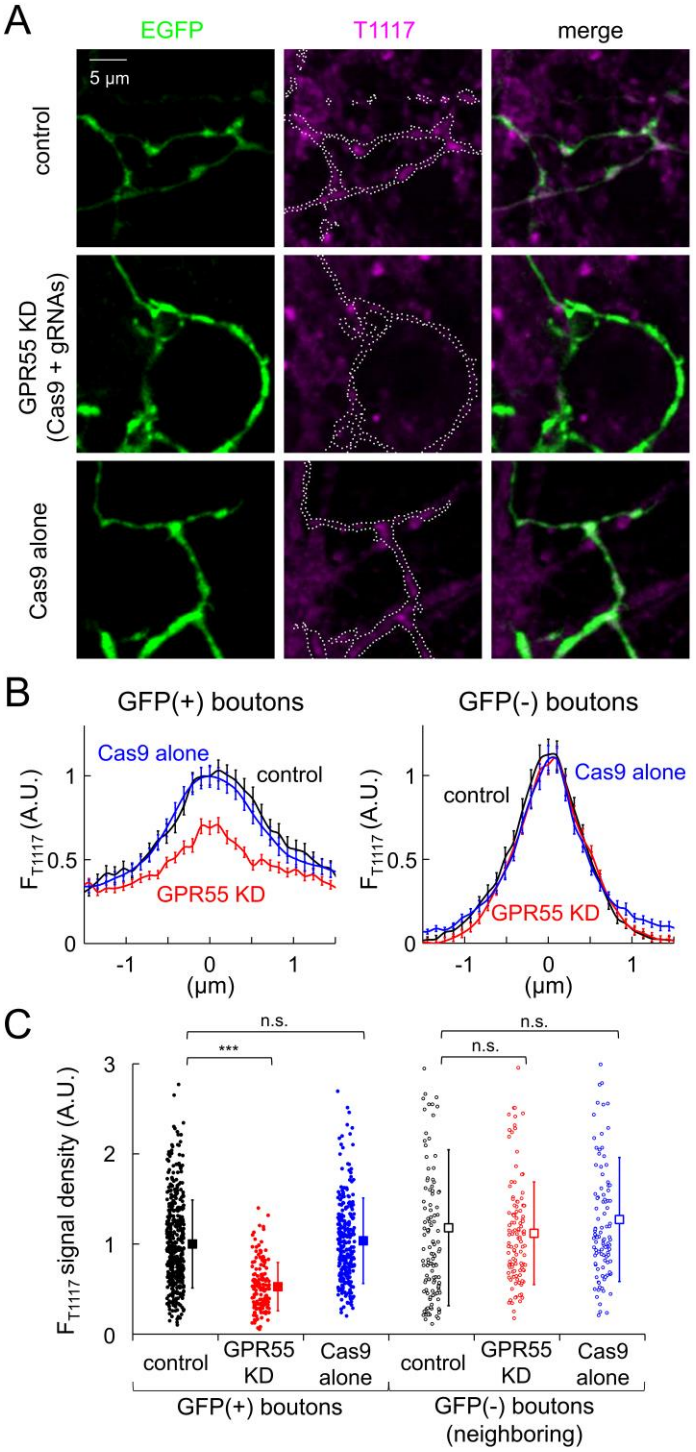

Figure 2. Localization of GPR55 at PC axonal boutons

(**A**) Representative confocal fluorescent images of GFP and T1117 labeling in control and transfected cells with GPR55-targeting CRISPR/Cas9 vectors or Cas9-alone. White dotted lines in the T1117 images indicate the outlines of GFP-labeled axons. (**B**) Spatial profiles of T1117 signals in GFP(+) or GFP(-) boutons. Averaged data are shown as mean ± SEM. Fluorescence peak of GFP (for GFP(+) boutons) or T1117 (for GFP(-) boutons) was aligned to the position 0. (**C**) F_{T1117} signal density (averaged fluorescence per pixel) in GFP(+) boutons (control, 455; GPR55-KD, 161; Cas9-alone, 270 boutons) or that in GFP(-) boutons near GFP(+) ones (control, 124; GPR55-KD, 116; Cas9-alone, 104 boutons). Data for individual boutons (circles) and mean ± SD (squares) are shown. ***, $p < 0.001$; n.s., not significant.

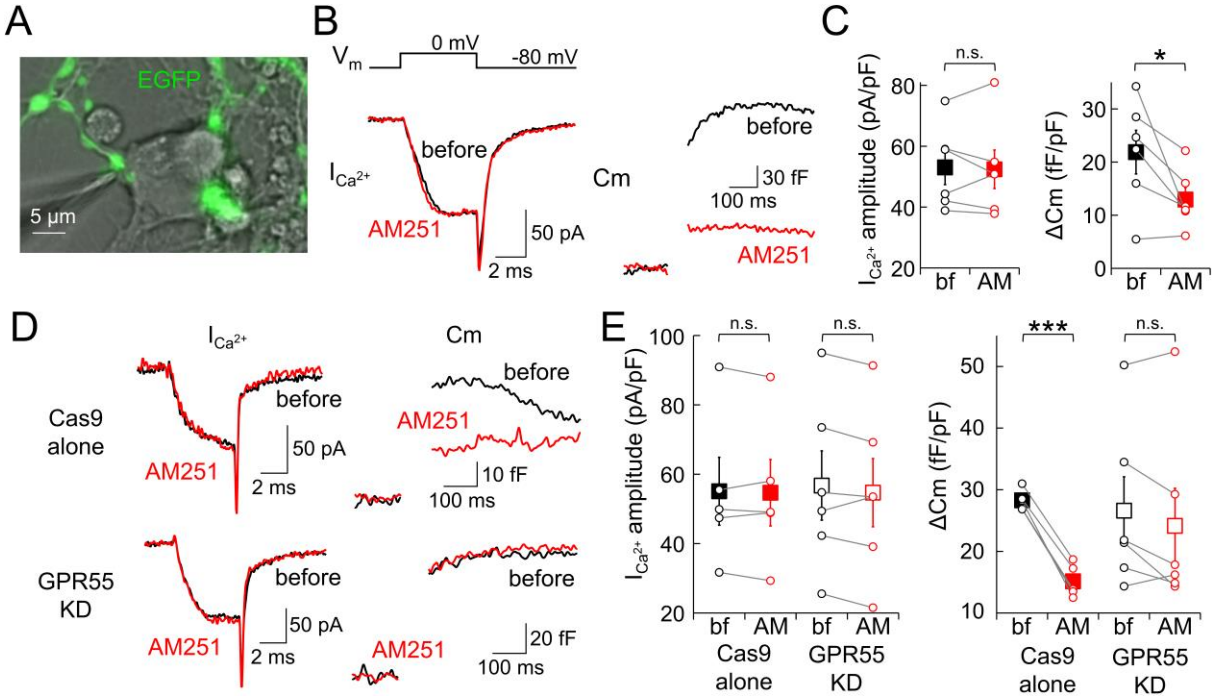

Figure 3. Reduced vesicle exocytosis by GPR55 without changing presynaptic Ca^{2+} influx
(A) Image of direct patch-clamp recording from an EGFP-labeled PC axon terminal in culture. (**B-E**) Representative traces (B, D) and amplitude of presynaptic Ca^{2+} currents during 5 ms depolarization ($I_{Ca^{2+}}$) and the resultant C_m increase (ΔC_m, C, E) before and after the AM251 application in wild-type (n = 6) (B, C) or transfected cells with Cas9-alone (n = 5), or CRISPR/Cas9 for GPR55 (n = 6) (D, E). Both $I_{Ca^{2+}}$ and ΔC_m were normalized by the size of presynaptic C_m under the voltage-clamp. The internal solution contained 0.5 mM EGTA. Data are mean ± SEM. * $p < 0.05$; *** $p < 0.001$; n.s., not significant.

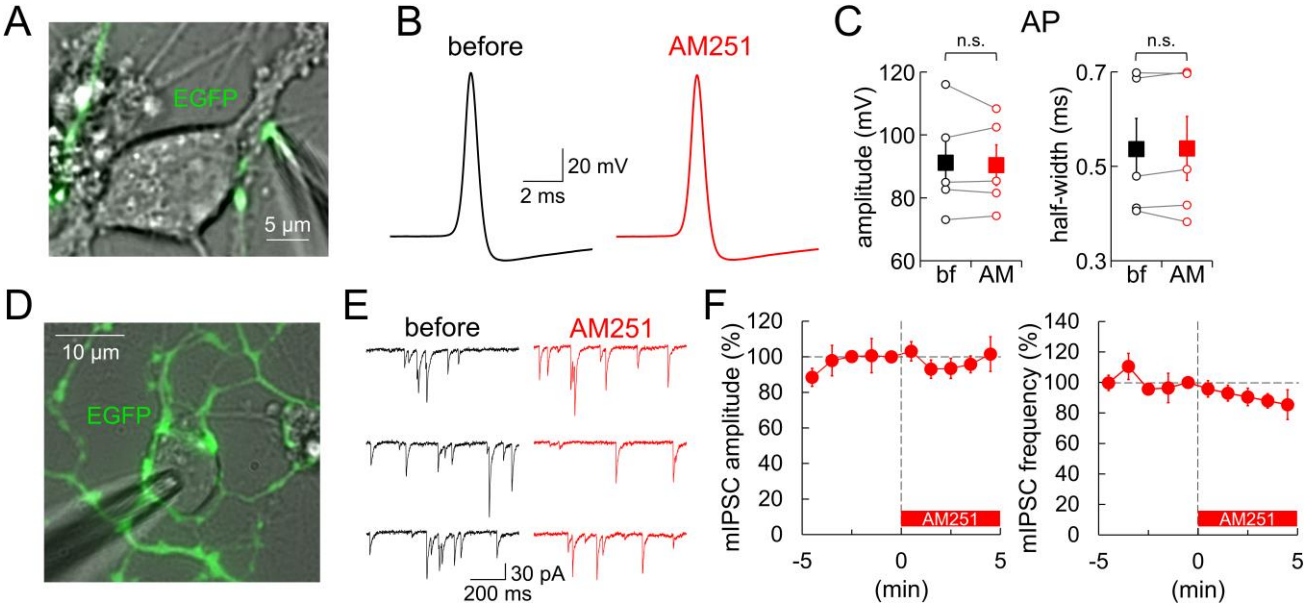

Figure 4. GPR55 has no effect on APs or postsynaptic responsiveness

(**A**) Image of direct recording from an EGFP-labeled PC axon terminal in culture. (**B, C**) Representative traces (B), amplitude and half-width (C) of APs recorded from PC terminals before and 5 minutes after the AM251 application (n = 5). (**D**) Image of mIPSC recordings from a neuron innervated by lots of EGFP-positive PC boutons in culture. (**E**) Representative traces of mIPSCs before and 5 minutes after the AM251 application. (**F**) Time courses of mIPSC amplitude and frequency (n = 4). At 0 min, AM251 was applied. The internal solution contained 0.5 mM EGTA. Data are shown as mean ± SEM. n.s., not significant.

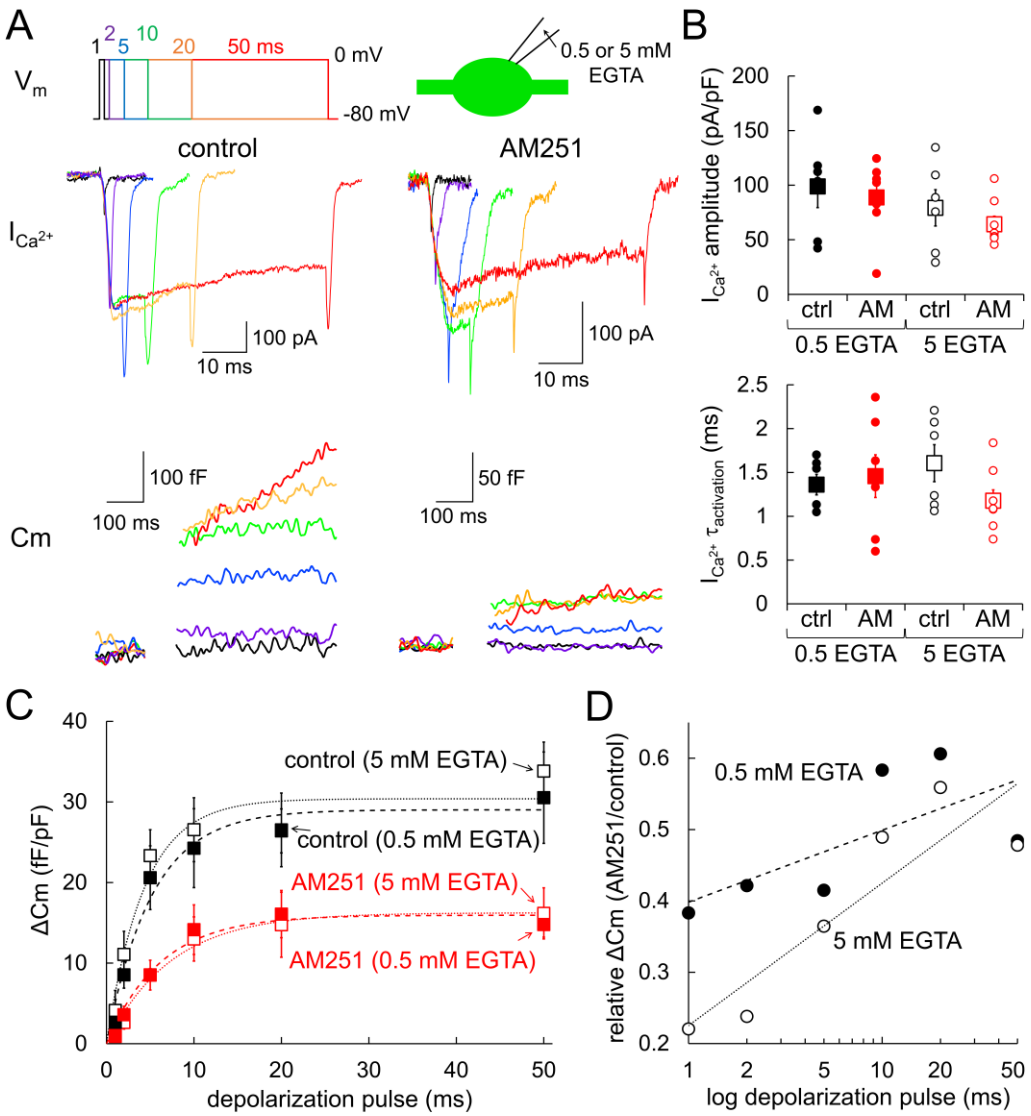

Figure 5. Decrease in RRP vesicles by GPR55

(**A**) Representative traces of presynaptic $I_{Ca^{2+}}$ (middle) and the resultant C_m increase (bottom) recorded with presynaptic 0.5 mM EGTA upon 1, 2, 5, 10, 20, or 50 ms of depolarization pulses (to 0 mV) (top) without (left) or with (right) AM251. Experiments were performed with a presynaptic patch pipette containing 0.5 mM or 5 mM EGTA. (**B**, **C**) Amplitude and time constant for activation of $I_{Ca^{2+}}$ (B), and C_m change (C) upon depolarization pulses recorded without (black, 0.5 mM EGTA, n = 6; 5 mM EGTA, n = 6) or with AM251 (red, 0.5 mM EGTA, n = 7; 5 mM EGTA, n = 8). Single exponential fits for each are shown as dotted lines. Both $I_{Ca^{2+}}$ and C_m change were normalized by the size of presynaptic C_m under the voltage-clamp. In B, data for individual cells (circles) and mean ± SEM (squares) are shown. (**D**) Ratio of C_m increase (C_m increase with AM251 divided by that in control) recorded with 0.5 or 5 mM presynaptic EGTA is plotted against the logarithm of pulse duration.

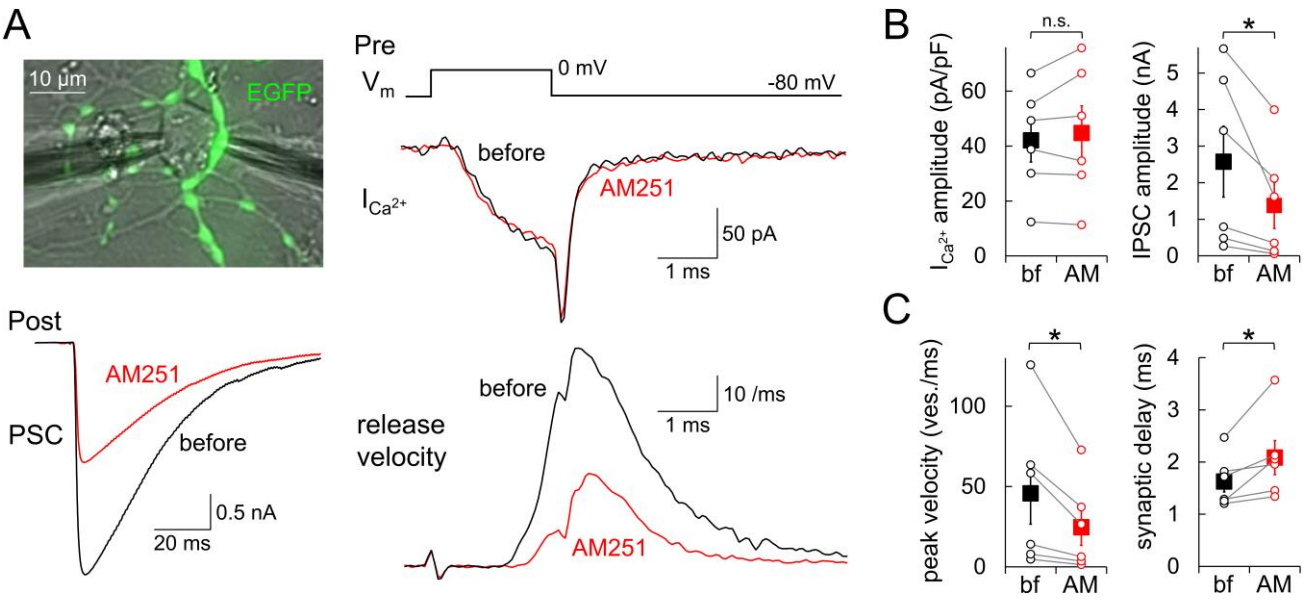

Figure 6. Halved velocity of exocytosis shown by pre- and postsynaptic paired recordings (**A**) Image of paired recordings from a presynaptic EGFP-labeled PC bouton and its postsynaptic neuron (upper left), and representative traces of the presynaptic $I_{Ca^{2+}}$ (upper right), IPSC (lower left), and velocity of vesicular fusion (bottom right; calculated by the deconvolution of IPSC trace) upon 2 ms depolarization before and after the AM251 application. (**B, C**) Amplitude of $I_{Ca^{2+}}$ (B, left, calibrated by the presynaptic C_m under the voltage-clamp), IPSC (B, right), maximal release velocity (C, left) and synaptic delay (C, right) before and after application of AM251. The internal solution contained 0.5 mM EGTA. Data are mean ± SEM. * $p < 0.05$; n.s., not significant. n = 6 pairs.

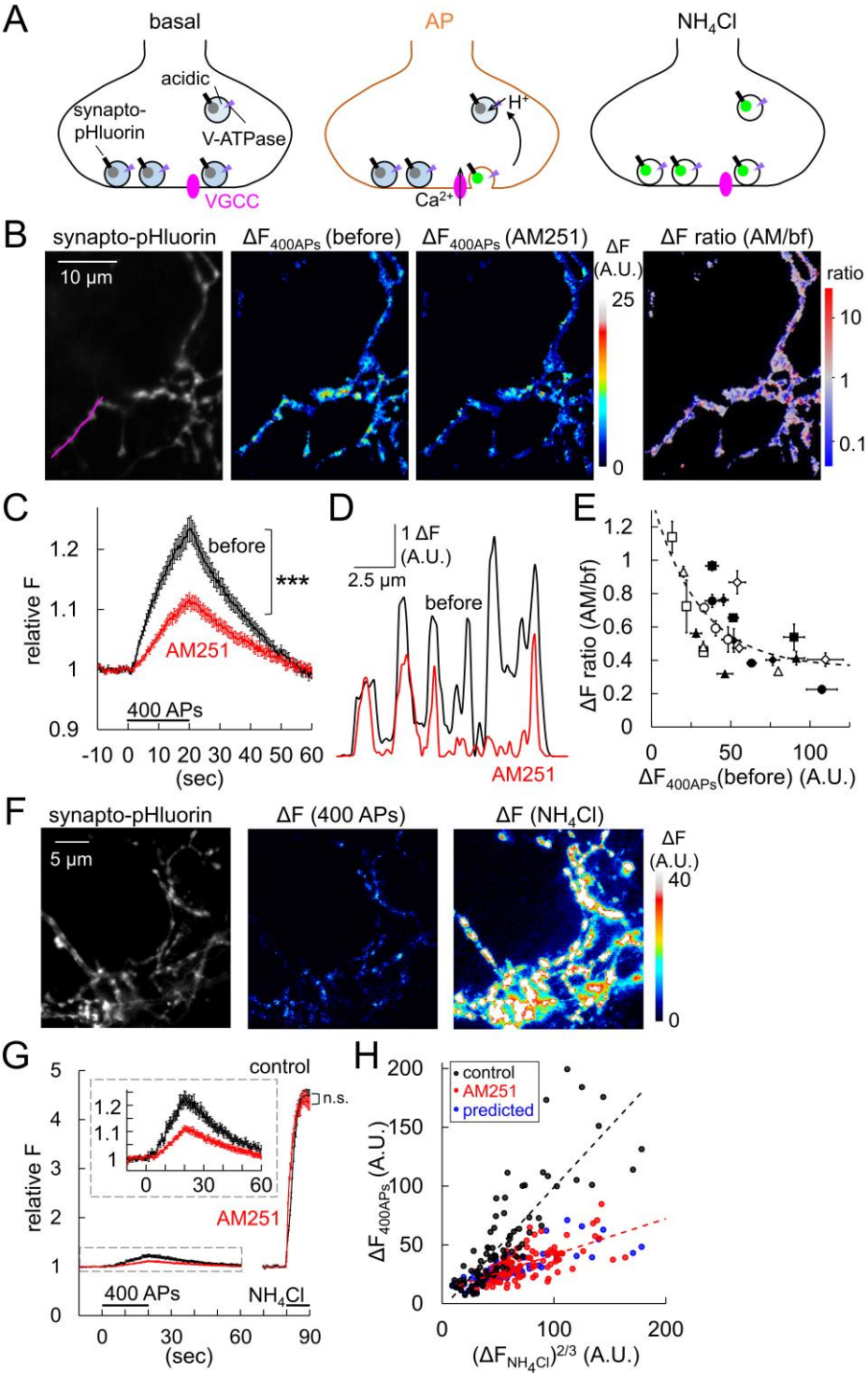

Figure 7. Halved vesicular releases by GPR55 imaged with pHluorin

(**A**) Schematic illustration for imaging of vesicle exocytosis with synapto-pHluorin. Upon vesicular fusion at the AP arrival, pHluorin becomes fluorescent because of exposure to the neutral pH. NH_4^+ application forcefully neutralizes vesicle lumen. (**B**) Representative images of synapto-pHluorin fluorescence and the color-coded fluorescence increase upon 400 APs (ΔF_{400APs}) in PC terminals before and after the AM251 application. The right-most panel shows the ratio of fluorescence increase after the AM251 application relative to that before, represented in pseudo-color. (**C**) Time courses of 400 APs-triggered pHluorin fluorescence changes before and after the AM251 application. (**D**) Plot of ΔF_{400APs} along a PC axon (indicated as a magenta line in B) before and after the AM251 application. (**E**) Ratio of ΔF_{400APs} after the AM251 application relative to that before is plotted against the ΔF_{400APs}

976 before the AM251 application. Data from different cells are shown as different symbols. n = 8 cells.
977 Dashed line represents data fitting with a function: $y = 1.02e^{-0.0334x} + 0.355$, $R^2 = 0.506$. (**F**) Images of
978 pHluorin fluorescence and the color-coded fluorescence increases in a PC axon upon 400 APs and
979 the following NH_4Cl application (50 mM). (**G**) Time courses of synapto-pHluorin fluorescence changes
980 upon 400 APs and the following NH_4Cl application without or with AM251. Inset shows enlarged
981 traces. (**H**) ΔF_{400APs} is plotted against the 2/3rd of ΔF caused by NH_4Cl (ΔF_{NH4Cl}) for individual boutons
982 without or with AM251. The effect of AM251 was predicted (blue) by conversion of dataset for control
983 (black) based on the relationship shown in E, showing similar distribution to the actual data obtained
984 with AM251 (red). Fitted line for control: $y = 1.03x – 4.05$, $R^2 = 0.704$; for AM251, $y = 0.307x + 10.9$,
985 $R^2 = 0.441$. Data are mean ± SEM. *** $p < 0.001$; n.s., not significant.

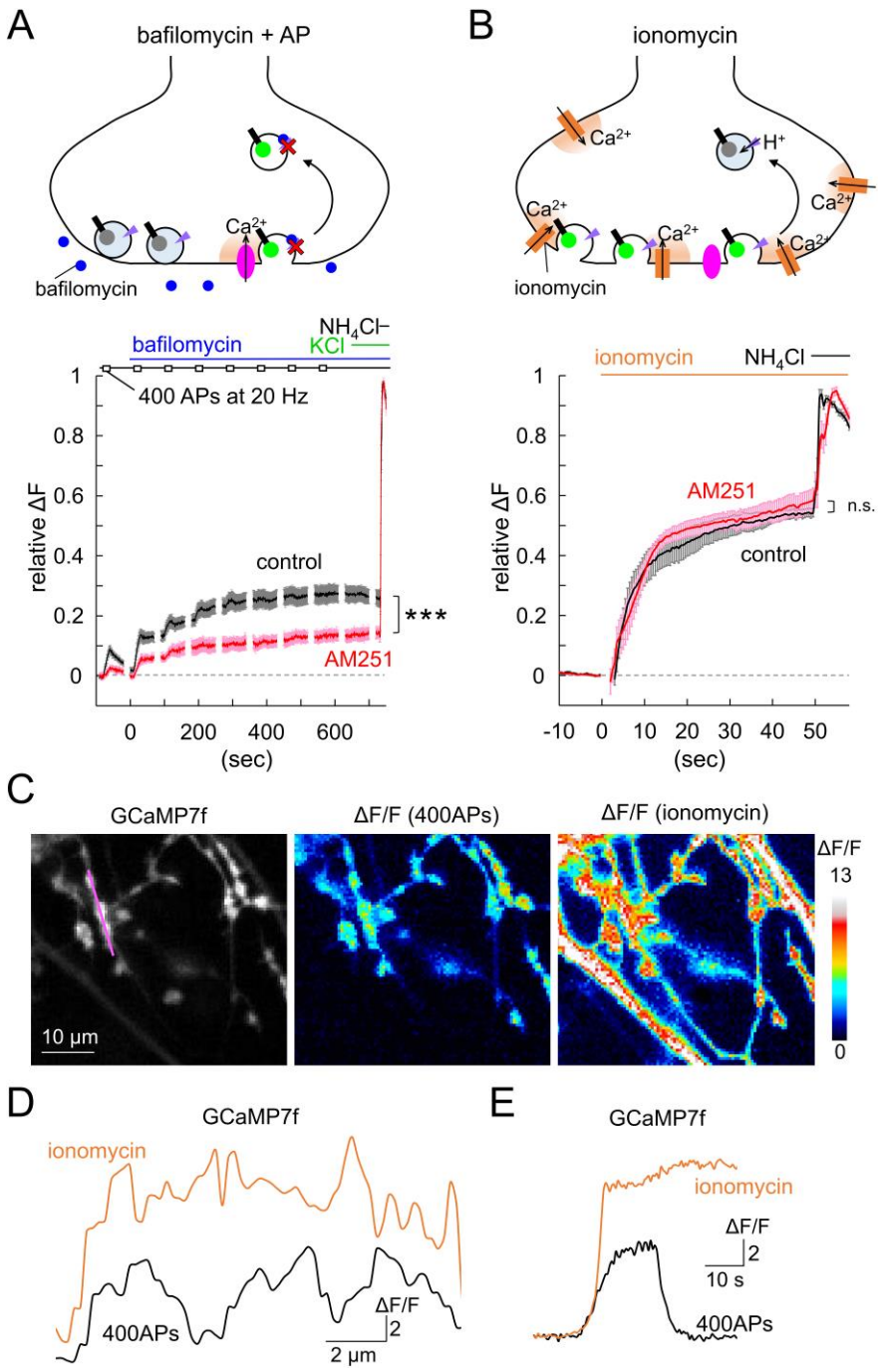

Figure 8. Increase in reluctant vesicles insensitive to APs by GPR55

(**A, B**) Schematic illustration (top) and time courses of synapto-pHluorin fluorescence changes at PC axon varicosities upon the repetitive 400 APs trains (20 Hz) before and after the application of bafilomycin and KCl (finally 50 mM) (A), or ionomycin (B), followed by the NH_4Cl application, in the presence or absence of AM251. Data are mean ± SEM. *** $p < 0.001$; n.s., not significant. (**C**) Fluorescent images of GCaMP7f expressed in PC axon terminals (left) and color-coded relative fluorescence increase (ΔF/F) upon 400 APs at 20 Hz (middle) or the following ionomycin application (right). (**D, E**) Distribution patterns along an axonal segment (D; indicated as the magenta line in C) or representative time courses (E) of ΔF/F caused by 400 APs or ionomycin.

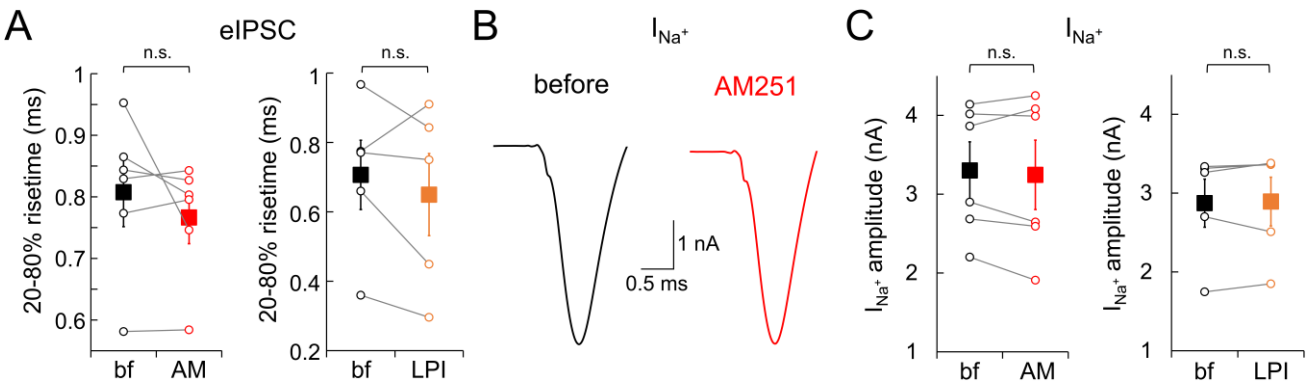

Figure 1—figure supplement 1. No effects of GPR55 on IPSCs time courses and somatic Na^+ currents

(**A**) 20-80% risetime of eIPSCs before and after application of AM251 or LPI. Data for individual cells are also shown (open circles). (**B, C**) Representative traces (B) and amplitudes (C) of Na^+ current before and after application of AM251 or LPI. AM251, n = 6; LPI, n = 5. Data are mean ± SEM. n.s., not significant.

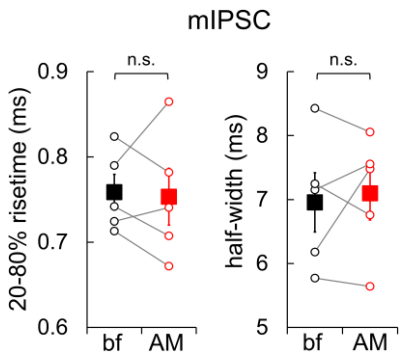

1003

1004 **Figure 4—figure supplement 1. No effects of GPR55 on time courses of mIPSCs**

1005 20-80% risetime or half-width of mIPSCs before and after application of AM251 (n = 5). Data for

1006 individual cells are also shown (open circles). Data are mean ± SEM. n.s., not significant.

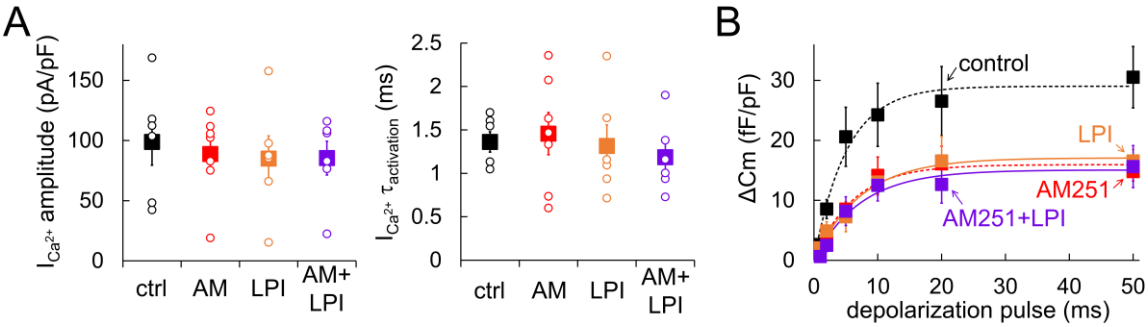

Figure 5—figure supplement 1. AM251 and LPI occlude the suppressive effects on vesicle release each other

(**A**, **B**) Amplitudes and time constants for activation of presynaptic $I_{Ca^{2+}}$ (A), and C_m changes (B) upon depolarization pulses recorded with LPI only (orange, n = 6) or with LPI and AM251 (purple, n = 6). For comparison, control and AM251 data (shown in Figure 5) are also presented. Single exponential fits for each are shown as dotted or solid lines. Both $I_{Ca^{2+}}$ and C_m change were normalized by the size of presynaptic C_m under the voltage-clamp. In A, data for individual cells (open circles) and mean ± SEM (squares) are shown. The presynaptic internal solution contained 0.5 mM EGTA.

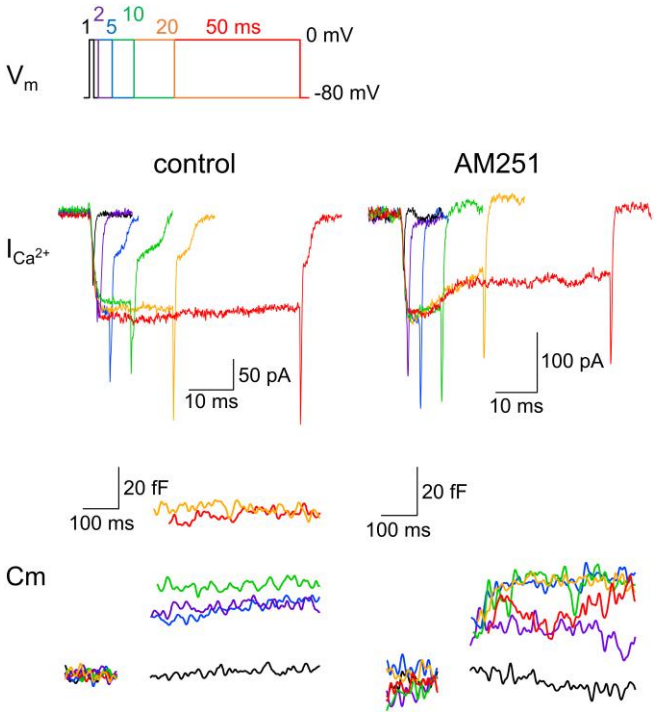

Figure 5—figure supplement 2. GPR55-mediated suppression of release in PC boutons with 5 mM EGTA

Representative traces of presynaptic $I_{Ca^{2+}}$ (middle) upon 1, 2, 5, 10, 20 and 50 ms of depolarization (to 0 mV, depicted on the top) of a PC bouton, and the resultant C_m increase (bottom) in the presence or absence of AM251. Recording was performed with a patch pipette containing 5 mM EGTA.

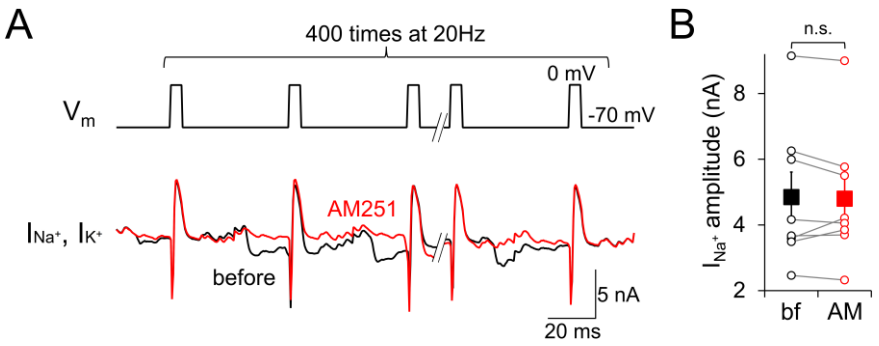

Figure 7—figure supplement 1. No effects of GPR55 on somatic Na^+ currents upon repetitive stimulation at 20 Hz

(**A**) Representative traces of Na^+ and K^+ currents before and after application of AM251. (**B**) Amplitudes of Na^+ current upon repetitive stimulation at 20 Hz before and after application of AM251 (n = 7). Data for individual cells are also shown (open circles). Data are mean ± SEM. n.s., not significant.

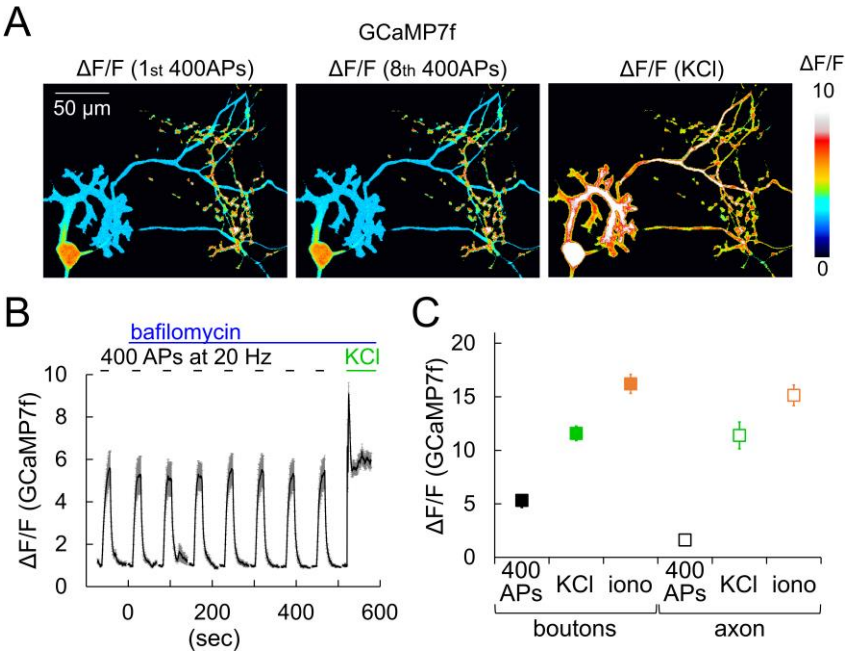

Figure 8—figure supplement 1. Ca^{2+} influx induced by AP trains, external high K^+ or ionomycin

(**A**) Color-coded relative fluorescence increase of GCaMP7f (ΔF/F) upon 400 APs at 20 Hz (at the 1_{st} round or the 8_{th}) or the following KCl application (finally 50 mM). (**B**) Time course of GCaMP7f ΔF/F upon the repetitive 400 APs trains and KCl before and after application of bafilomycin. (**C**) GCaMP7f ΔF/F at boutons on axons upon 400 APs, application of KCl or of ionomycin (iono). n = 35 (400APs), 10 (KCl) and 20 (ionomycin) boutons, or 41 (400 APs), 15 (KCl) and 26 (ionomycin) sites in axon. Data are mean ± SEM.